2D-1D Semiconductor Heterostructures: Synthesis, Characterisation and Optoelectronic Applications

ANG JIAN MARTIN

A0087255X

A THESIS SUBMITTED FOR THE FULFILLMENT FOR THE DEGREE IN BACHELOR OF SCIENCE (HONOURS)

DEPARTMENT OF PHYSICS

NATIONAL UNIVERSITY OF SINGAPORE

AY2014/15

Acknowledgements

This Final Year Project is indeed an experience to remember. This journey had its excitements and disappointments. It has given me a glimpse into the life of a researcher, experiencing both the frustration that come with setbacks, and the joy that come from breakthroughs. There are many people along the way who have given me invaluable help and support. Without them, doing this project would be become exponentially tougher.

First of all, I would like to thank my supervisor, Professor Sow Chorng Haur, for all his guidance through my project. Being the Head of Department for Physics, he was always very busy. However, he always managed to make time to drop by and ask us how we were and how our projects were doing. He would listen and then guide us to what the next appropriate cause of action should be. He also had this amazing ability to explain difficult concepts in a surprisingly simple way, which made learning under him a lot easier. This was something I found very fascinating as I am planning to become a teacher myself. I am very glad to have had him as my supervisor.

I would also like to thank my mentor, Lu Junpeng, for walking us through this project, taking the time out to sit down with us each day to check our progress and advising us accordingly. I am very thankful for him teaching me how to use the equipment in the lab, as well as explaining concepts to me.

I also would like to thank the others in my lab for being such pleasant people to be with. Not only are they very friendly to talk to and joke around with every once in a while, but everybody is also so willing to help each other, be it helping to troubleshoot a problem with equipment or even just looking for a specific thing in the messy old lab. All this helps in creating a very warm and welcoming environment at the lab. It was something that I noticed within the first few weeks of my project, and it is something that I treasure.

Lastly, I would also like to thank my family and friends for supporting me through this time. Friends were also good to talk to during the struggles with the project as many of them could empathise with me, especially the other year 4 students. After a day of experiments that gives you results that just do not make sense to you, and feeling lost, it is always a very comforting thing to come back to a family that loves you.

Table of Contents

1. Abstract

2D materials have become very popular in recent years in the electronics industry. This is due to the unique properties of a 2D material compared to its bulk form. In my project, Chemical Vapour Deposition (CVD) is used to fabricate 2D Transition Metal Dichalcogenides (TMDs) on either a Sapphire or Silicon dioxide (SiO_2/Si) substrate. The characteristics of these TMD flakes are studied through the use of different techniques. Raman Spectroscopy is used to identify the TMD. Photoluminescence Spectroscopy helps determine its bandgap. Atomic Force Microscopy allows me to study the morphology of the TMD flake. Fluorescence Microscopy helps determine the specific areas of fluorescence on the TMD flake. This is followed by a manual stacking of a Cadmium Selenium Sulfide, $CdS_{0.8}Se_{0.2}$, nanowire. This forms a heterostructure junction. This junction is made into an optoelectronic device. Lasers of different wavelengths were incident upon the junction through global irradiation and the photoelectrical properties, such as Photoresponsivity, External Quantum Efficiency (EQE) and Photodetectivity, were studied using graphs of current against voltage (IV) and current against time (Ivst).

2. Introduction

Many 2D materials have been used as the building blocks for electronic devices all over the world. A lot of research has been done in recent years to study the properties of these 2D materials. Some examples of these 2D materials are Graphene, Boron Nitride and Transition Metal Dichalcogenides (TMDs).

However, many of these materials face difficulties in being used in optoelectronics. Graphene for example, has a zero bandgap[1]. Although this means that the conductivity of graphene is excellent, it also implies that the charge carriers do not have any significant large excitations or relaxations to absorb or emit fluorescence or PL. Boron Nitride on the other hand, has a bandgap that is too large. The bandgap is 5.97eV[2], which corresponds to a wavelength of 208nm, which is in the ultraviolet range of the electromagnetic spectrum. This large bandgap causes boron nitride to have a very low conductivity and behave as an insulator and is used as a dielectric in some cases. Although most of the 2D TMDs have a bandgap corresponding to the visible light range, some TMDs have a low mobility due to the reduction in the amount of charge carriers compared to its bulk form.[3] However, through the use of heterostructures, we might be able to overcome some of the disadvantages which individual materials possess.

2.1. Project Description

The first stage of this project was to do a parameter search for the synthesis of thin TMD flakes on different substrates. I will be focusing on synthesizing thin WS_2 flakes on both sapphire and SiO_2/Si substrates. For synthesis, the Chemical Vapour Deposition (CVD) technique chosen, using WO_3 and Sulphur powders as precursors and argon gas as the carrier gas. Repeated experiments were done to find the optimum conditions for synthesis.

The second stage of this project was to study the characteristics of the WS_2 flakes synthesized. This was done using 4 different techniques. Raman Spectroscopy was used to identify WS_2, Photoluminescence Spectroscopy to determine the bandgap, Atomic Force Microscopy to study the morphology and Fluorescence Microscopy to determine the specific areas of fluorescence on the flake.

The final stage of this project is to study the optoelectronic properties of heterostructures. The two materials chosen were WSe_2 and $CdS_{0.8}Se_{0.2}$. The reason for this choice was to develop a *p-n* heterostructure junction. These two materials can also be synthesized using the CVD technique. The heterostructure junction was made using the Electron Beam Lithography (EBL) technique and placed on a Side-Brazed Dual In-line Ceramic Package (DIP). This optoelectronic device was used to measure the photocurrent of the heterostructure junction through IV and Ivst plots using lasers of different wavelengths. The Photoresponsivity, External Quantum Efficiency (EQE) and Photodetectivity were calculated using these measurements. These values were compared with that of non-heterostructure junctions.

2.2. Transition Metal Dichalcogenides (TMDs)

Atomically thin sheets of TMDs are a promising class of materials for a range of applications.[4] These materials are made to complement or even replace certain standard materials being used in semiconductor devices currently.[5] One reason for this is due to the direct bandgap the 2D TMDs possess. The concept of a direct bandgap is illustrated in the diagram below.

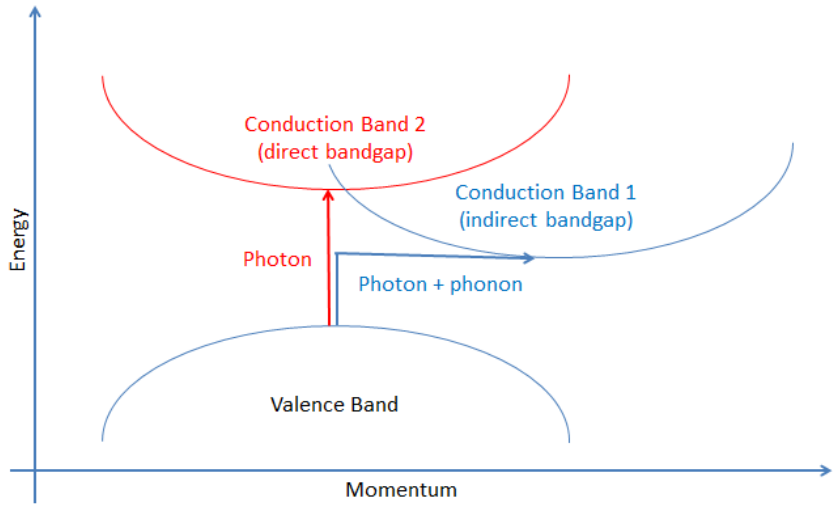

Fig 1: Energy profile diagram of direct and indirect bandgaps

Bulk TMDs possess an indirect bandgap. This means that for an electron to transfer from the valence band to the conduction band, a photon and a phonon is needed, as illustrated in the figure above. However, when a TMD monolayer is used instead, the bandgap changes to a direct bandgap.[6] This means that only a photon is needed for the excitation of an electron.

This allows the material to exhibit fluorescence and photoluminescence which is useful for optoelectronics.

Thin 2D TMDs can be synthesized by a few methods. The exfoliation technique can be used, where a thin layer of TMD can be mechanically cleaved off of a bulk TMD using an adhesive tape. This is possible due to the structure of TMDs.[4] Similar to graphene, TMDs consists of layers of covalent bonds. This can be seen in the figure below which shows the monolayer structure for MoS_2.

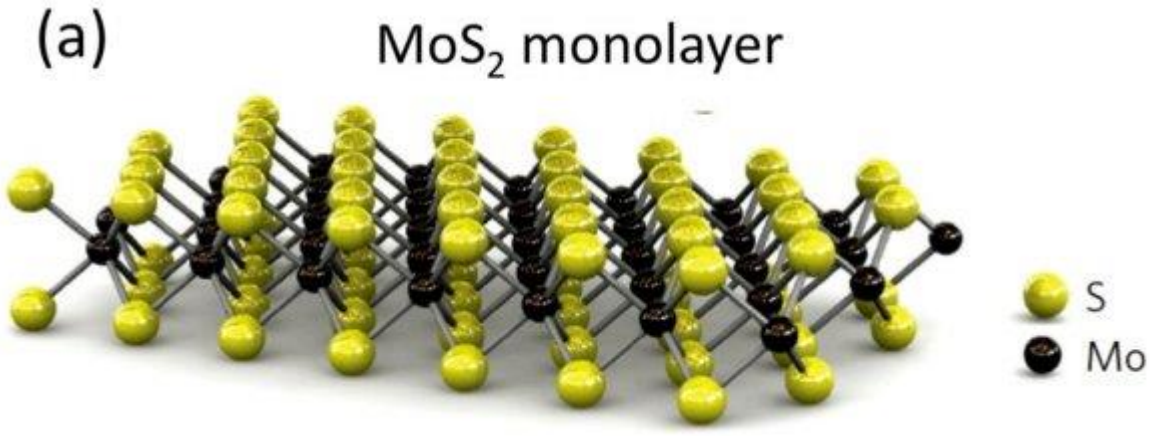

Fig 2: Atomic structure of monolayer MoS_2. (© Johnny Wong, University of Twente)

In a bulk TMD, the monolayers are bonded to each other through weak Van Der Waals forces.[4] This explains why the exfoliation technique is appropriate in synthesizing thin 2D TMDs. However, this technique has a low yield and has little control over the thickness of the TMD flake obtained.[7]

In my project, I will be using the Chemical Vapour Deposition technique to synthesize 2D TMDs. This technique will be elaborated in the following section of my report.

2.3. Chemical Vapour Deposition (CVD)

There are many different variations and modifications that can be applied to CVD. However in my project, I will be using a standard Atmospheric pressure CVD. Below is a diagram showing the different processes during CVD.

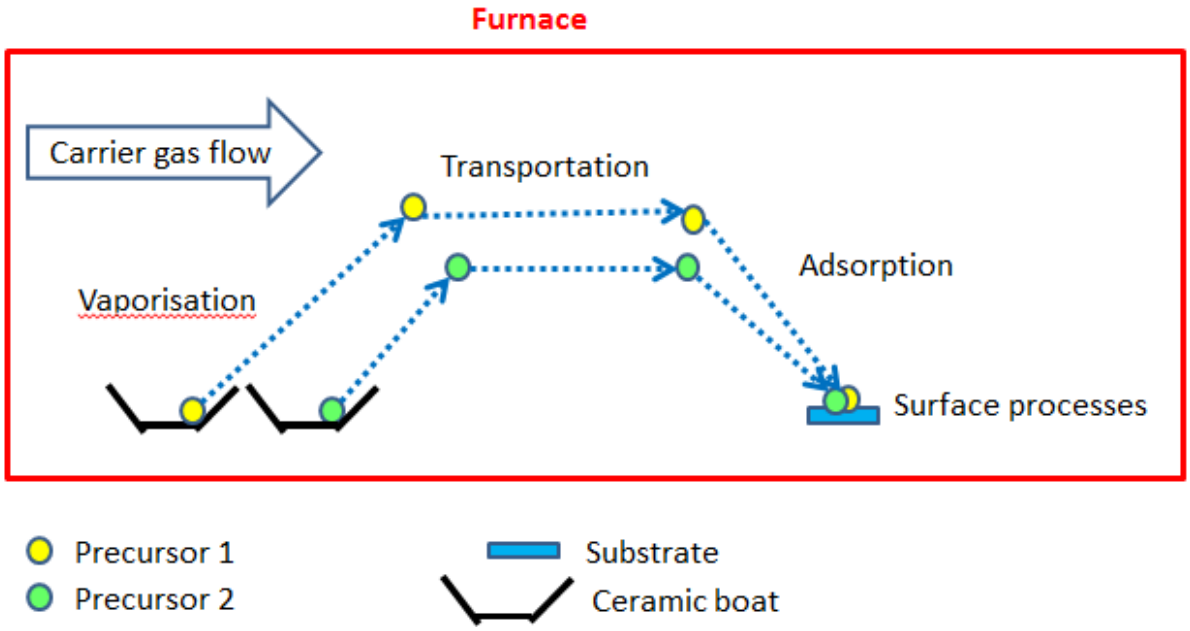

Fig 3: Diagram of processes in CVD

The diagram shows the precursors and substrate being placed in a furnace. The furnace has an input of carrier gas. When the temperature is high enough, the precursors begin to vaporize. The precursors are then transported by the carrier gas to the substrate which is placed downstream of the furnace. The precursors are then adsorbed onto the surface of the substrate. On the surface, the precursors can undergo several surface processes such as nucleation and surface diffusion. Through this CVD, various different thin film materials can be synthesized with the use the appropriate precursors.

2.4. *p-n* junction

Semiconductors conduct electricity through the presence of charge carriers within them. The two possible charge carriers are electrons and holes. To explain these charge carriers, the example silicon will be used.

Silicon is a group IV element, meaning it has 4 electrons in its outer shell. In a pure silicon crystal, the atoms are bonded to each other through covalent bonds, each atom having 4 bonds. When an electron in a bond gains enough energy, it can break free of its bond and become a charge carrier. This also creates a ‘hole’ at its initial electron position.

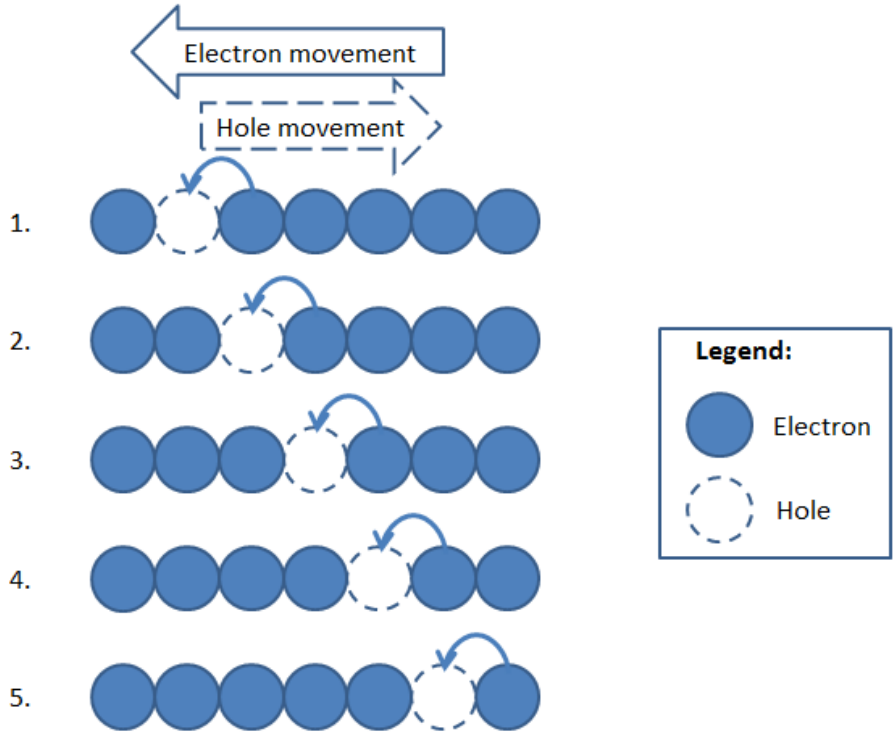

Fig 4: Diagram of movement of hole within semiconductor

This hole can be filled up by other nearby electrons. However, when a nearby electron takes up the position of this hole, the position which the electron came from will now be a hole. This phenomenon is illustrated in the diagram above. Although a hole is just the absence of an electron and does not carry a charge itself, the presence of this hole allows the nearby electrons to move and therefore creates a current. It should be noted that the flow of electrons in one direction would cause the hole to flow in the opposite direction.

Some semiconductor materials intrinsically have extra free electrons or holes which increases its conductivity. Free electrons and holes can also be introduced into a semiconductor through doping, which is the addition of impurities. A semiconductor which has more free electrons than holes is called an n-type semiconductor. A semiconductor with more holes than free electrons in called a p-type semiconductor. When these 2 types of semiconductors are placed adjacent to each other, a *p*-*n* junction is formed.

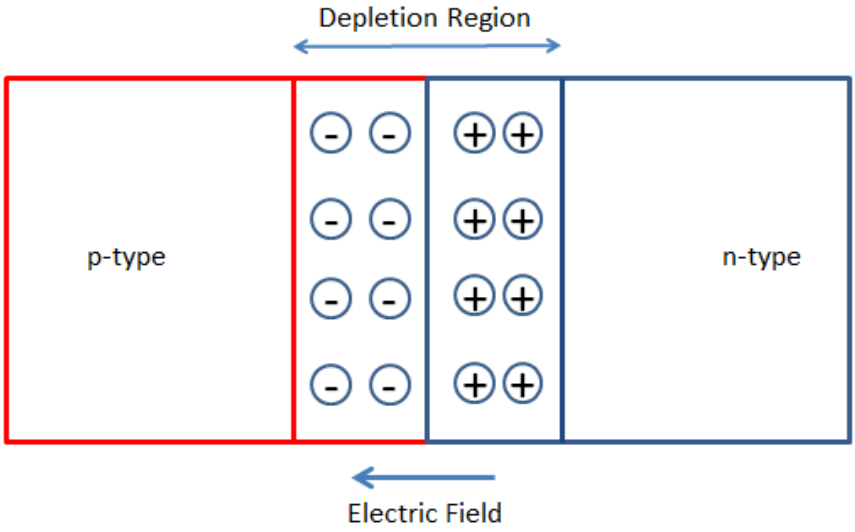

Fig 5: *p-n* junction diagram

The above diagram shows what happens in a *p-n* junction. The excess electrons from the n-type semiconductor combine with the excess holes in the p-type semiconductor for annihilation. However, this process leaves behind positive ions in the n-type semiconductor and negative ions in the p-type conductor. These remaining ions then create an electric field that hinders free electrons from diffusing into the p-type region. This diffusion occurs until the electric field is stronger enough to prevent further diffusion. The region of positive and negative ions is called the depletion region, where the charge carriers are depleted.

A potential difference can be applied across the junction, where the positive terminal is placed at the p-type semiconductor and the negative terminal at the n-type semiconductor. If the potential difference is larger than the electric field in the depletion region, the electrons can overcome the electric field barrier and travel from the n-type to the p-type semiconductor, thus resulting in a current through the junction. This is called a forward bias.

However, if the potential difference is applied in the other direction, where the positive terminal is placed at the n-type region and the negative terminal at the p-type region, the electric field at the depletion region is now enhanced even further, creating an even larger depletion region. There is no current through the junction in this case. This is referred to as a reverse bias.

This shows that a *p-n* junction behaves as a diode, allowing current to flow in the forward bias direction but not in the reverse bias direction.

3. Methodology

3.1. Synthesis of WS_2 through Chemical Vapour Deposition (CVD)

The CVD method was used to grow WS_2 flakes on different substrates. One tube furnace was used for sapphire substrates and another tube furnace was used for Silicon dioxide (SiO_2/Si) substrate.

3.1.1. Furnace used to synthesize WS_2 on SiO_2/Si

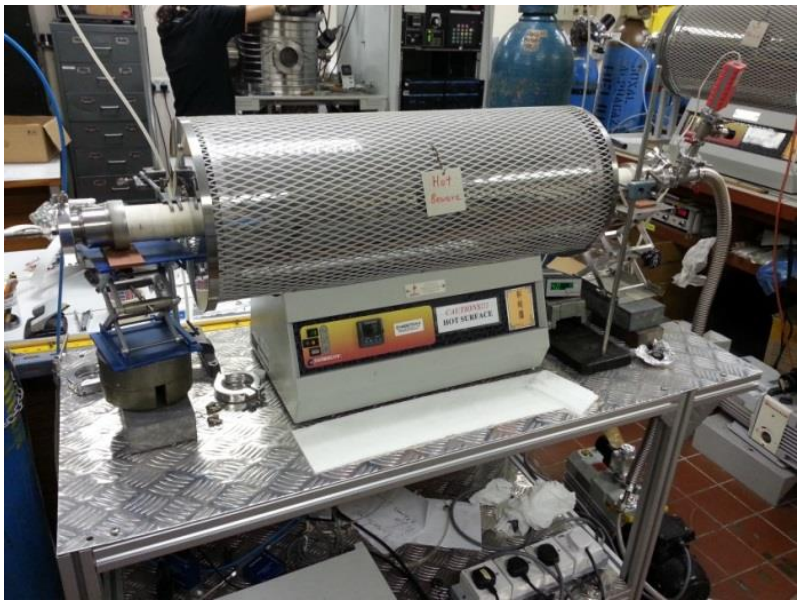

Fig 6: Furnace used to grow WS_2 on SiO_2/Si substrate

The cross section of the furnace used to synthesize WS_2 on SiO_2/Si is displayed in the diagram below.

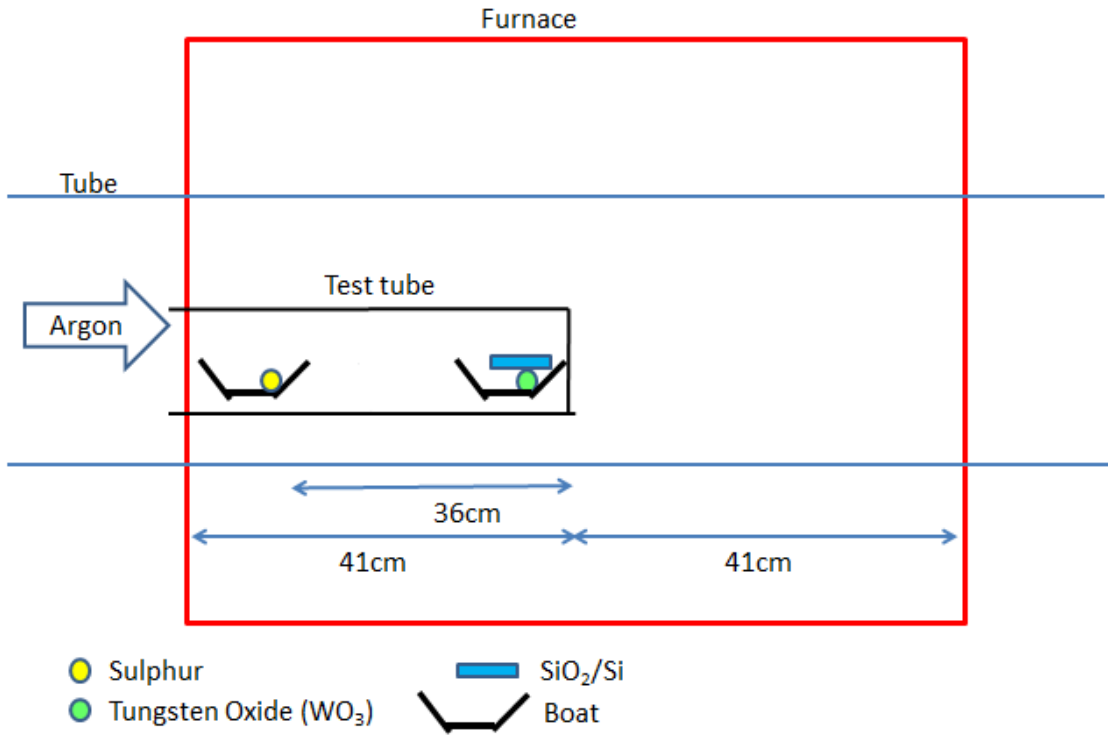

Fig 7: Cross section of furnace used to synthesize WS_2 on SiO_2/Si

WO_3 and Sulphur precursor is placed in a ceramic boat each, along with the SiO_2/Si substrate. These ceramic boats are then placed in a test tube within the tube furnace. An argon gas canister is attached to the inlet of the tube furnace. The rate of gas flow is controlled by a mass flow controller. The outlet can either be connected to a vacuum pump to achieve lower pressures, or connected to an open tube, keeping the pressure in the tube furnace at atmospheric pressure.

According to Ling et al.[8], using a seeding promoter such as perylene-3,4,9,10-tetracarboxylic acid tetrapotassium salt (PTAS) on SiO_2/Si substrate enhances the synthesis of MoS_2 through Chemical Vapour Deposition. The PTAS molecular aggregates act as seeding promoters and initiate the growth of thin layer MoS_2 flakes. In my experiment, I made a PTAS solution using a concentration 50μM, stated in a paper written by Lee et al.[9] and dropcast it onto the SiO_2/Si substrate, followed by drying through heating at 80˚C.

The furnace is then set run a certain temperature setting.

3.1.2. Furnace used to synthesize WS_2 on Sapphire

Another furnace with a slightly differing setup was used to synthesis WS_2 on Sapphire.

Fig 8: Furnace used to grow WS_2 on Sapphire

The cross section of the furnace is as such.

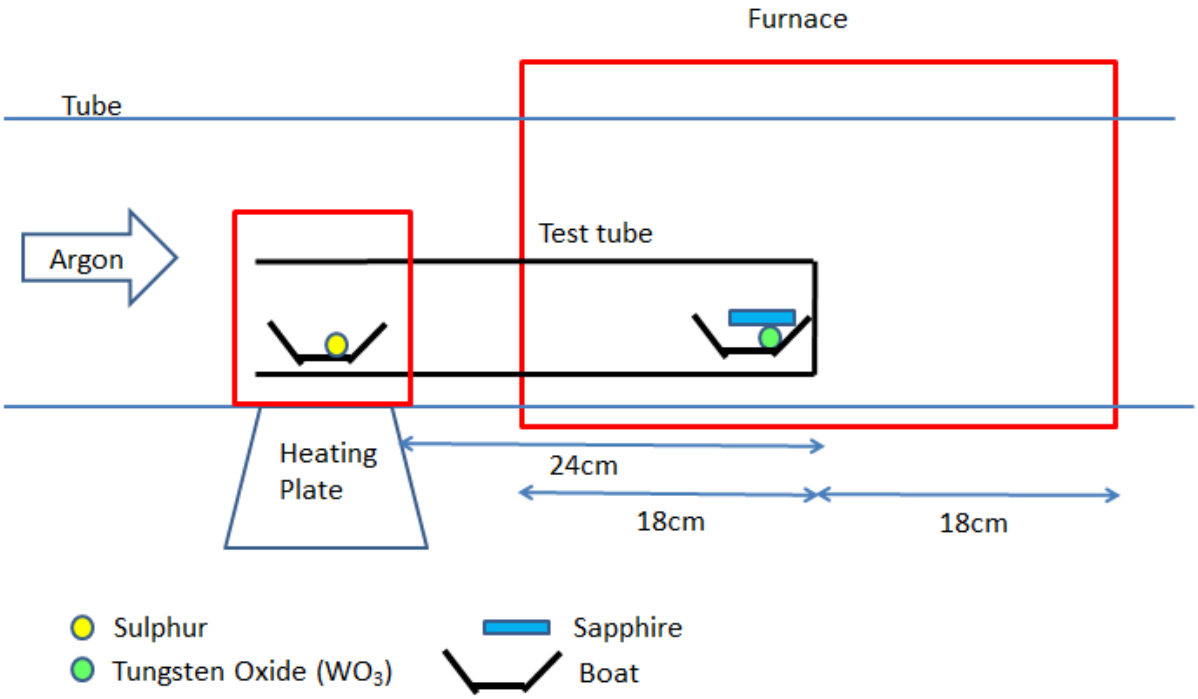

Fig 9: Cross section of furnace used to synthesize WS_2 on Sapphire

The setup of this furnace is very similar to the furnace used to synthesize WS_2 on SiO_2/Si. However, instead of having the Sulphur precursor boat being in the furnace, it is placed outside the furnace, under a heating plate. The heating plate helps to control the temperature of the Sulphur separately. The Sulphur was heated to a temperature of 290˚C. According to Peimyoo et al.[10], heating the Sulphur separately helps in a more uniform growth of the WS_2 flakes.

The gas flow was also controlled by a mass flow controller and the outlet was also open to the atmospheric pressure.

The furnace is then set run a certain temperature setting.

3.2. Characterisation of WS_2

I used 4 techniques to study the WS_2 flakes synthesized. The four techniques are Raman Spectroscopy, Photoluminescence Spectroscopy, Fluorescence Microscopy and Atomic Force Microscopy. Each of these methods helps us to study an aspect of the WS_2 flakes.

3.2.1. Raman Spectroscopy

Raman Spectroscopy is a method used to study the molecular vibrational and rotational modes of a sample through Raman Scattering.

Fig 10: Raman Microscope used for Raman Spectroscopy

In Raman Spectroscopy, a monochromatic laser beam is incident onto the sample. In my case, the excitation wavelength used was 532nm. Majority of the photons will be elastically

scattered, also known as Rayleigh scattering, which means that they will be the same wavelength as the incident photons. However, there will be a small portion of photons which will be inelastically scattered, which is called Raman Scattering. This is due to the laser photons interacting with the molecular vibrations of the sample. Raman Scattering wavelengths deviate from the excitation wavelength to extents, depending on the vibrational modes present. This gives each material a specific Raman spectrum.

Often after a synthesis process, there are many microscopic objects of different shapes and sizes on the substrate that can be seen optically. Raman spectroscopy can also be used to identify and confirm what is seen.

The graphs of Raman Spectroscopy plot the Intensity of scattered photons against the shift in wavenumber with respect to the incident photon's wavenumber.

3.2.2. Photoluminescence (PL) Spectroscopy

According to Gfroerer[11], PL is the spontaneous emission of light from a material under optical excitation. PL Spectroscopy is a non-destructive method used to study the optical properties of a material. A photon of a higher frequency and energy is incident onto the sample. For my PL Spectroscopy, I used an excitation wavelength of 532nm to incident onto the WS_2 flake. This photon causes electrons in the material to excite to a higher energy level, overcoming its bandgap. Following this, the electron will undergo relaxation processes. The relaxation across the bandgap will occur as an emission of a photon, which is the PL observed. PL Spectroscopy plots the intensity of PL detected against wavelength. PL Spectroscopy helped to determine the bandgap of the WS_2 flake.

3.2.3. Atomic Force Microscopy (AFM)

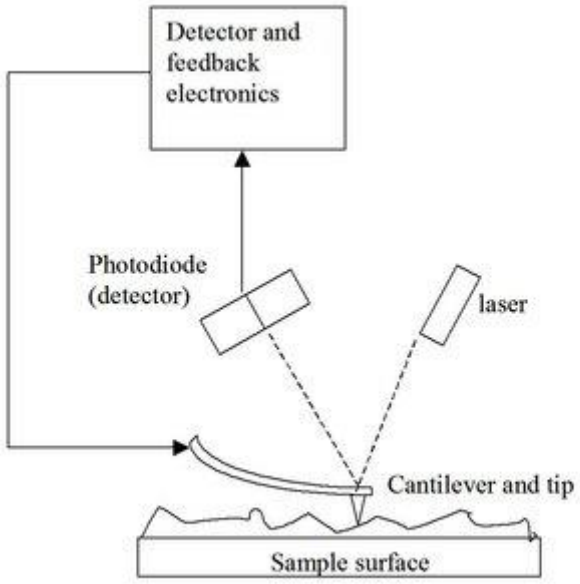

Fig 11: Setup of Atomic Force Microscopy. (© Edinformatics.com)

Tapping mode Atomic Force Microscopy (AFM) is a method used to study the morphology of a material's surface. The setup is as shown above. A cantilever and tip are used as a probe to map out the surface of the sample. When the tip is brought close to the surface, various different forces between the surface and the tip will cause the angle of deflection of the laser to change. These deflections are detected by a photodiode acting as a detector. The photodiode will then feedback to the system to adjust the tip-to-sample distance. This is to prevent the tip from being damaged by the surface. These changes will correspond to the height of the point on the surface, which is then recorded. The cantilever will go back and forth along the surface and slowly plot out the morphology of the surface.

3.2.4. Fluorescence Microscopy

Fluorescence Microscopy is commonly used in today's research, especially in the fields of Biology. It is very good for visual detection and tracking of certain cells which might exhibit specific fluorescence. Certain dyes can be used to coat certain materials for easy tracking. Fluorescence occurs when photons of a higher energy, compared to that of the bandgap of a material, is incident onto the material. If the photon is within the absorption range of the material, the photon will excite the electron into a higher energy state. The electron will then

release energy through photons and other forms of vibrations. The photon emitted by the electron when dropping back down the bandgap is the fluorescence seen. This is very similar to PL mentioned earlier. In Fluorescence Microscopy however, an optical image of the fluorescence is taken rather than an intensity plot of fluorescence. This helps us to visually see which points on the WS_2 flake emit fluorescence.

3.3. Optoelectronic Device

An optoelectronic device was made to study the properties of the junction through IV and Ivst graphs. WSe_2 flakes were used instead of WS_2 flakes. The reason for this choice will discussed in section 4.3.

3.3.1. Fabrication of Optoelectronic Device

First, Polymethyl Methacrylate (PMMA) is applied onto the substrate containing the WSe_2 flake. It is spin coated and then baked. This material polymer is used as a photoresist. After a layer of PMMA is formed, the substrate is put into an EBL chamber where the electron beam is used to draw out the position desired for the electrode. According to Choi et al.[12], the electron beam causes chain scission within the PMMA which degrades it. The substrate is then placed in photoresist developer which dissolves away only the degraded PMMA. Following this the substrate is washed with DI water and dried with Nitrogen gas. The substrate is then put into a thermal evaporator with 2 heating sources within it, one with Gold (Au) and the other Palladium (Pd). A layer of Palladium of 20nm thick is deposited on the substrate followed by 80nm of Gold. Following this, Acetone is used to remove the remaining PMMA on the substrate, leaving behind Pd/Au electrodes at the desired positions. The process is finished off by washing the substrate in DI water and dried with Nitrogen gas.

For my device in particular, a $CdS_{0.8}Se_{0.2}$ nanowire was stacked on top of a WSe_2 flake, as can be seen in the figure below.

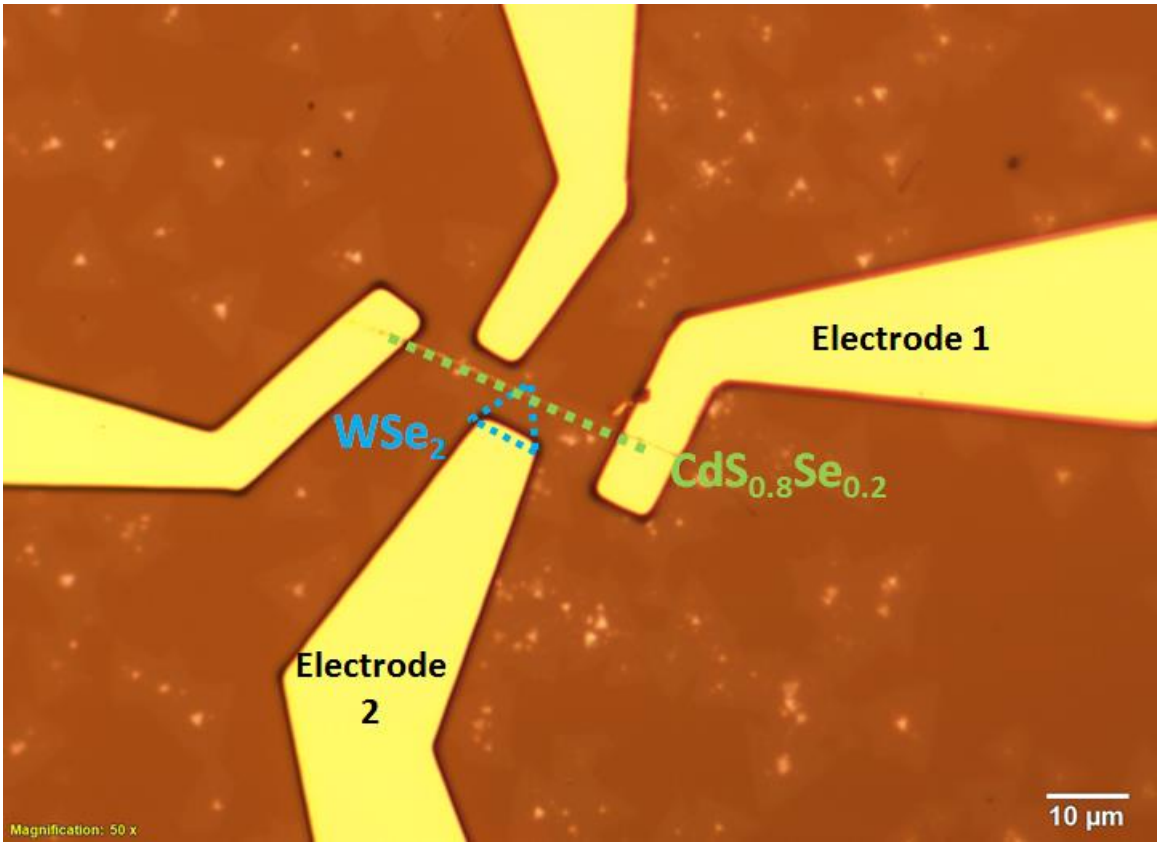

Fig 12: Optical image of Optoelectronic Device on a Sapphire substrate

The $CdS_{0.8}Se_{0.2}$ nanowire and WSe_2 flake was highlighted in green and blue for easier observation. The two electrodes of interest are labelled Electrode 1 and 2.

$CdS_{0.8}Se_{0.2}$ nanowire is also prepared using the CVD technique, except that the prescursors used are CdS and CdSe powder. The reason for using $CdS_{0.8}Se_{0.2}$ over CdS, CdSe or even $CdS_{0.65}Se_{0.35}$ is that $CdS_{0.8}Se_{0.2}$ has the better optoelectronic properties such as a higher "ON/OFF" ratio.[13]

The substrate is then placed in a Side-Brazen Dual In-line Ceramic Package (DIP) where the electrodes can be electrically connected to copper wires for easier use, as can be seen in the picture below.

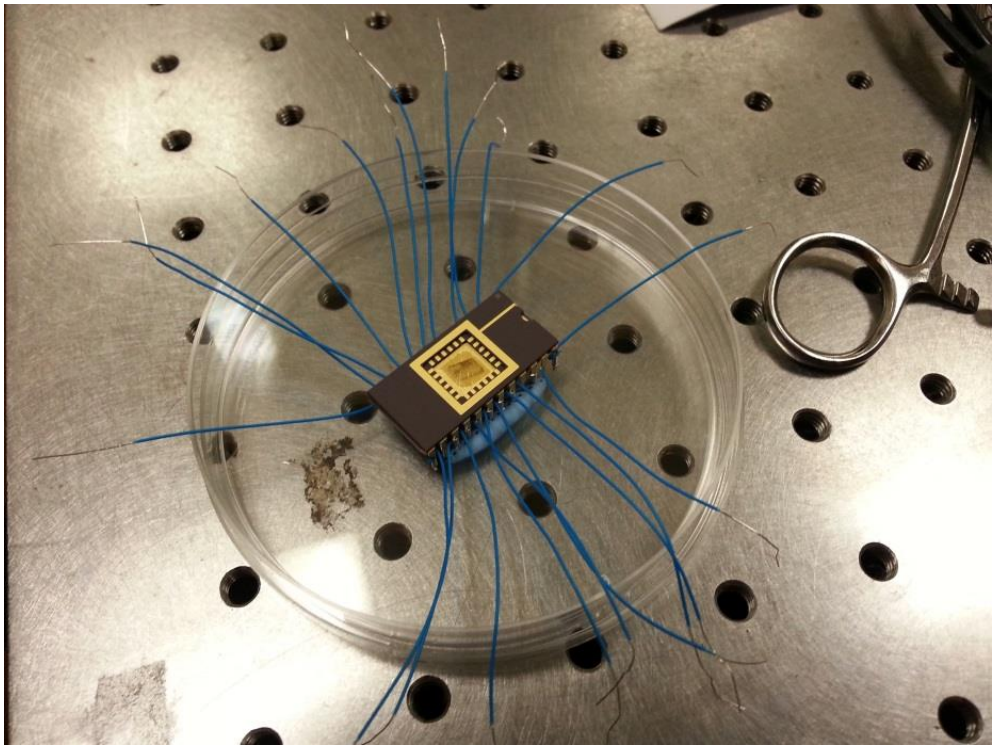

Fig 13: DIP containing sapphire substrate in the centre

3.3.2. Measuring Photocurrent

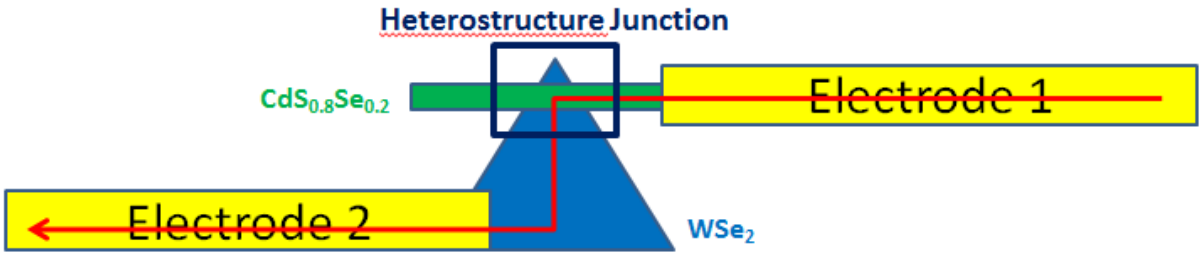

Fig 14: Schematic diagram of heterostructure junction

Above is the setup on the optoelectronic device. The current runs through Electrode 1, through the $CdS_{0.8}Se_{0.2}$ nanowire, pass the heterostructure junction into WSe_2 and then through Electrode 2.

The electrodes are connected to a sourcemeter which provides a sweeping DC bias voltage and measures current simultaneously. The measurements were done at room temperature and in ambient conditions. Different broad beam lasers were being used for the measurements.

The lasers were mounted on a tripod stand and incident upon the substrate, ensuring that the entire heterostructure junction and the electrodes contact with the WSe_2 flake and $CdS_{0.8}Se_{0.2}$ nanowire are uniformly illuminated. This is called global irradiation. Measurements were done for both dark current and with laser incidence of different wavelengths.

Besides IV graphs, current against time (Ivst) graphs were measured as well. During the measurement, the laser used is being blocked and unblocked approximately every 5 seconds. The “ON” state refers to when the laser is unblocked and “OFF” when the laser is blocked. This way, the difference between dark current and the current under illumination can be measured.

4. Results

4.1. Synthesis of WS_2 with CVD

A majority of my time spent on this project was on doing parameter searches for the optimum conditions for growth of WS_2 on sapphire and SiO_2/Si. Approximately 160 CVDs were done in this project. It was very difficult to find optimum conditions as it was difficult to get consistent results with apparently the same parameters. It was probably the case that there were a few parameters I was unaware of that affected the growth of the TMD flakes. These parameters were not controlled and therefore leading to apparently inconsistent results. Across time, I did manage to find out a few of these parameters, but definitely not all. However, I did manage to find my best set parameters that have been giving me rather consistent growth for sapphire and SiO_2/Si substrates. Although definitely not with 100% consistency for good growth, this was the best set of parameters I could find out during my time doing this project.

4.1.1. Synthesis on SiO_2/Si substrate

There were many variations being made in the parameter search for synthesis of WS_2.

4.1.1.1. Position of substrate

The substrate was placed at different distances away from the WO_3 precursor within that ceramic boat for different CVDs. It was even placed at different positions in between the ceramic boats along the test tube. For the SiO_2/Si substrate, there is only 1 side which is used for the synthesis of TMD flakes. For many of these positions along the furnace, the substrate was tested both facing up and facing down. The size of the substrate was also varied for some of the positions. We discovered that the optimised position for the SiO_2/Si substrate was to place it face down, right above the WO_3 precursor, as shown in the figure below.

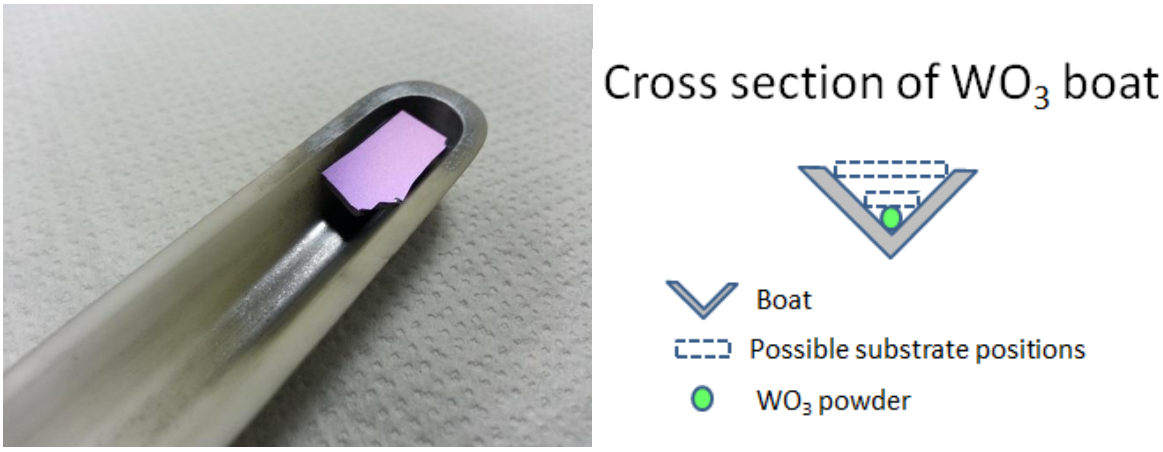

Fig 15: SiO_2/Si balanced in the boat right above WO_3 precursor

The WO_3 precursor, though cannot be seen in the picture, is below the SiO_2/Si substrate. The SiO_2/Si substrate is balanced above the precursor, supported by the sides of the boat. Due to the boat being V shaped, the substrate's distance above the WO_3 precursor can be altered by changing the width of the substrate, as can be seen in the "Cross section of WO_3 boat" diagram above. This made it difficult to obtain consistent results as the size of the substrate was altered through manual breaking. Breaking the substrate into the exact size and width desired required a lot of skill. The growth WS_2 flakes on the substrate is very sensitive to the height of the substrate above the WO_3 precursor. If it was too low, the WS_2 flakes would become thicker with more black particles covering it. These particles are suspected to be WS_2 particles, which are always seen in the ceramic boat after CVD, taking over the position of the WO_3 precursor. These particles however, cannot be removed by blow drying it with nitrogen gas. A picture of this is shown below.

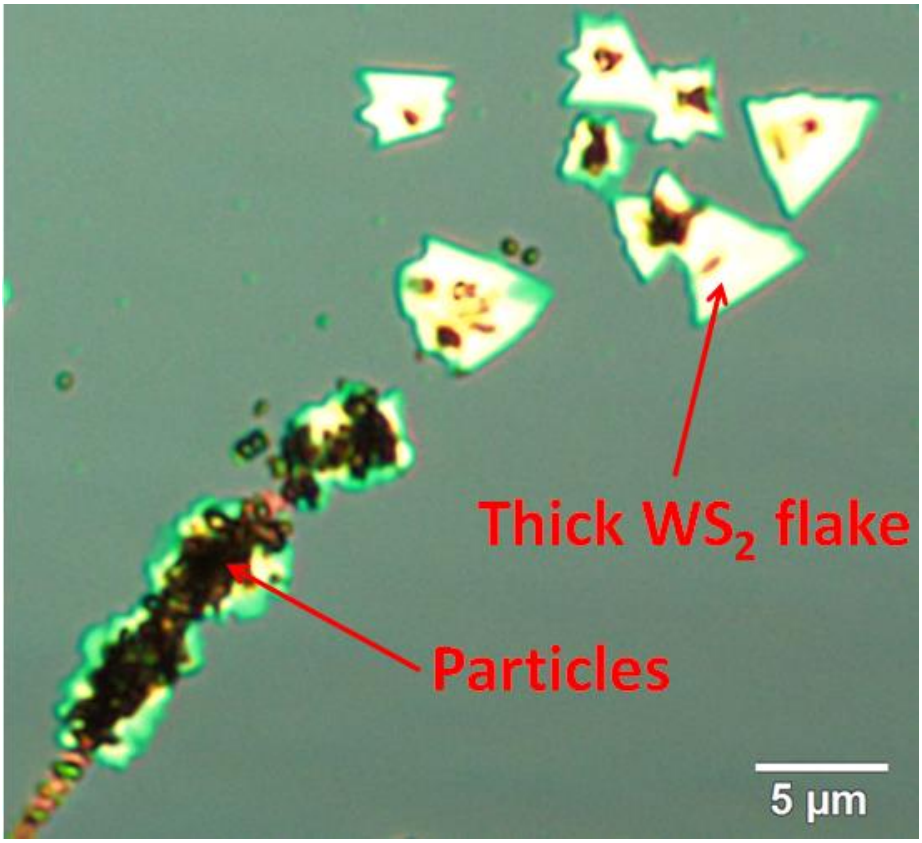

Fig 16: WS_2 particles and thick WS_2 flakes on SiO_2/Si

If it was too high, the WS_2 flake growth would be lesser and smaller. I found that the ideal height above the WO_3 precursor was approximately 2-3mm. 1mm would be too low and 4mm would be too high.

4.1.1.2. Position of precursor

The position of the precursor on the boats always remained the same. They were always placed at the corner of the boat, towards the side downstream of the furnace. The optimised positions of the ceramic boats were based on the temperature profile within the tube furnace.

The furnace does not experience a uniform temperature throughout its entire length. The edges of the furnace will experience a slightly lower temperature due to cooling from the environment outside the furnace. This is shown in the temperature profile diagram below.

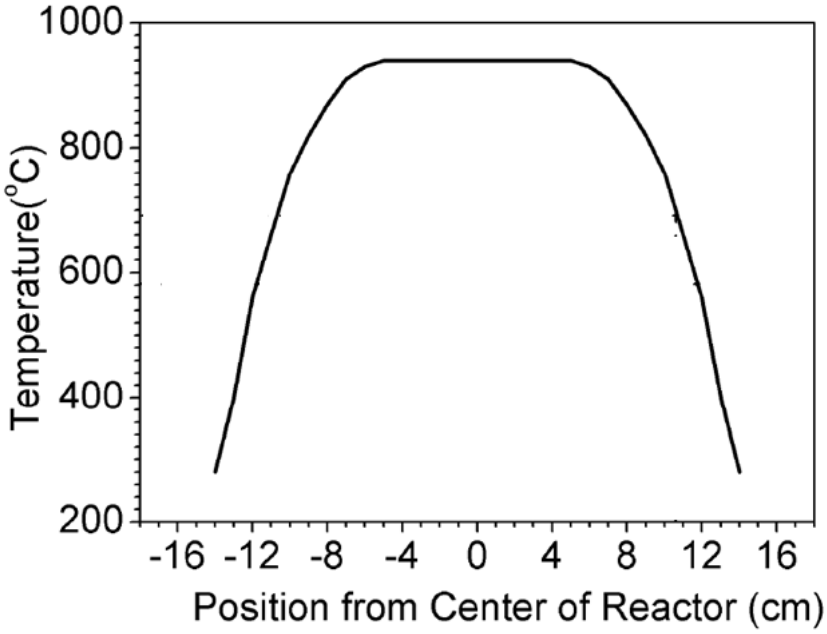

Fig 17: Temperature profile diagram of a similar tube furnace

This temperature profile was taken from a similar tube furnace of the same structure. The preset temperature was 950˚C, which was achieved at the centre portion of the furnace. Therefore, the boat containing the WO_3 precursor and the substrate are positioned such that the WO_3 precursor and substrate are aligned to the centre of the furnace. This is to ensure that the temperature the substrate and WO_3 precursor experienced was as close to the temperature settings as possible. The position of the sulphur boat is near the edge of the furnace, along the temperature gradient of the temperature profile, meaning that the temperature experienced is very dependent on the position of the boat. Through varying the position and comparing the growth of WS_2 flakes on the SiO_2/Si substrate, I found that if the Sulphur was placed too far away from the WO_3 precursor, there would be lesser growth. If I placed the Sulphur too near, the WS_2 flakes would be too thick. I experimentally found that the optimised distance between the centre of the furnace and the Sulphur precursor was approximately 36cm. This is illustrated in Fig 7 in section 3.1.1.

4.1.1.3. Amount of precursor

The amount of precursor was also experimentally optimised. For some of my synthesis processes, this was observed on my substrate.

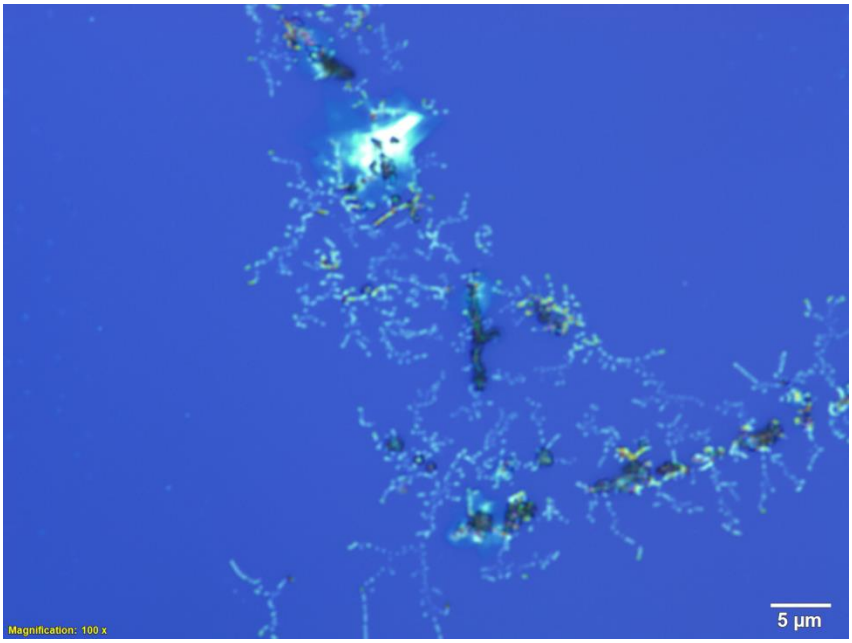

Fig 18: WS_2 nanowires

According to Rong et al.[14], these are WS_2 nanowires being formed. The formation of these nanowires indicates that the sulphur precursor is either introduced too late or there was not enough WO_3 precursor. For this furnace, the sulphur precursor was not separately heated from the WO_3 precursor, making it difficult to control how the sulphur precursor is heated without affecting the heating of the WO_3 precursor. Therefore, the amount of WO_3 precursor was altered instead. On the other hand, if there was too much sulphur precursor, the WS_2 flakes would be too thick. An image of thick WS_2 flakes can be seen in Fig 16 in 4.1.1.1. This knowledge made it a lot easier to optimise the amount of precursors needed for the CVD. The optimised amount of WO_3 was 20mg and sulphur was 240mg.

4.1.1.4. Temperature

The optimised temperature setting used is shown in the diagram below.

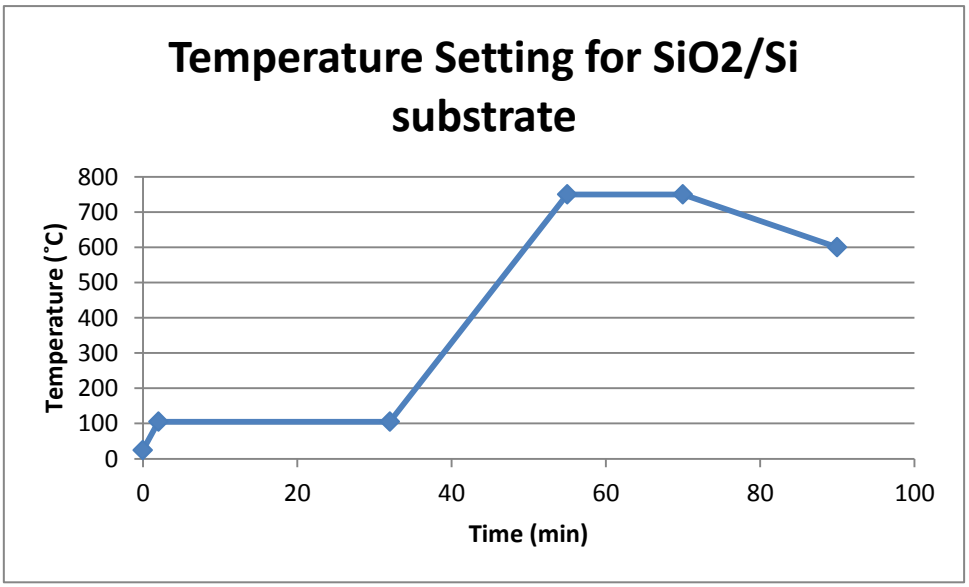

Fig 19: Temperature settings of furnace of SiO_2/Si

The temperature, starting at room temperature, was raised to 105˚C at a ramping speed of 40˚C/min and dwelled at that temperature for 30min. This was done so that all the air, water vapour and other impurities would be flushed out by argon gas. Following that, the temperature was raised to 750˚C at a ramping speed of 28˚C/min and dwelled at that temperature for 15min. The dwelling time is the growth stage for WS_2 flakes. Following that, the furnace was left to cool to room temperature by the argon gas flow and natural cooling.

The ramping speed leading to the growth stage was varied between 15-40˚C/min. Faster ramping speeds led to thicker flakes and slower speeds led to lesser flakes. The growth stage temperature was also varied between 600-850˚C. Both lower and higher growth stage temperatures led to lesser flakes. The growth stage time was also varied between 1 second to 40 min. It was difficult to observe a clear pattern for growth stage time as results were very inconsistent.

4.1.1.5. Gas supply and pressure

Throughout the whole process, the tube furnace is supplied with argon gas at 50sccm at room temperature and atmospheric pressure. At approximately 6 hours after the start of the CVD

process, the tube furnace would be approximately 350˚C. This is when the argon gas supply is stopped and the tube furnace is left to cool through natural cooling.

The rate of gas supply input was varied from 50-200sccm. Using faster rates led to thicker flakes. The pressure within the tube furnace was also varied between 0.57Torr to atmospheric pressure. Lower pressure was achieved through connecting the outlet of the tube furnace to a vacuum pump. Lower pressures led to lesser flake growth.

4.1.1.6. Cleaning substrate using Piranha solution

One of the suspicions for bad growth of WS_2 flakes was that the substrates used were not clean enough. Therefore, the substrates were washed in Piranha solution before using it for CVD. The Piranha solution consists of aqueous Sulphuric Acid and Hydrogen Peroxide. The concentrations of Hydrogen Peroxide and Sulphuric acid used were 30w/w and 98%w/w respectively. The ratio of volume of Sulphuric Acid to Hydrogen Peroxide was 3:1. The substrate was left inside the solution for approximately 16 hours. The substrates were then taken out, washed with DI water and dried with nitrogen gas. However, we found that this caused even less WS_2 growth. I speculate that it is because certain particles can acts as nucleation sites for the WS_2 flake. I did not use the Piranha solution in my ideal parameters for growth of thin WS_2 flakes.

4.1.1.7. Si_3N_4

In the later portion of my project, we tried to use the WS_2 flakes on SiO_2/Si substrate to make an optoelectronic device. However after running some tests, we realized that current could flow through SiO_2/Si surface itself, meaning that the current was not isolated to the WS_2 flake or $CdS_{0.8}Se_{0.2}$ nanowire. This meant that the dielectric layer on the SiO_2/Si was spoilt. We speculate that it is probably due to the high heat during the CVD process. I started using Si_3N_4 instead of SiO_2/Si for my CVD process, using the same parameters. There was successful growth of thin WS_2 flakes. However, I did not have time to make an optoelectronic device out of it due to time constraints.

4.1.1.8. Best Parameters

In summary, the best parameters I determined experimentally are as follows.

TMD grown:	WS_2	
Substrate used:	SiO_2/Si	
Position of substrate:	2-3mm above WO3, facing down	
Position of precursors:	WO_3: centre of furnace	Sulphur: 36cm upstream of centre
Amount of precursor:	WO_3: 20 mg	Sulphur: 240 mg
Gas supply & pressure:	Gas: 50 sccm argon	Pressure: 1 atm

Temperature settings		
End temp (°C)	**Ramping Speed (°C/min)**	**Time (min)**
105	40	2
105	0	32
750	28	55
750	0	70

Fig 20: Table of parameters for CVD on SiO_2/Si substrate

There were a lot of CVD carried out across the duration of my project. Approximately 80 CVDs were carried out for SiO_2/Si substrate.

Below are some optical images of the progress made across the duration of my project.

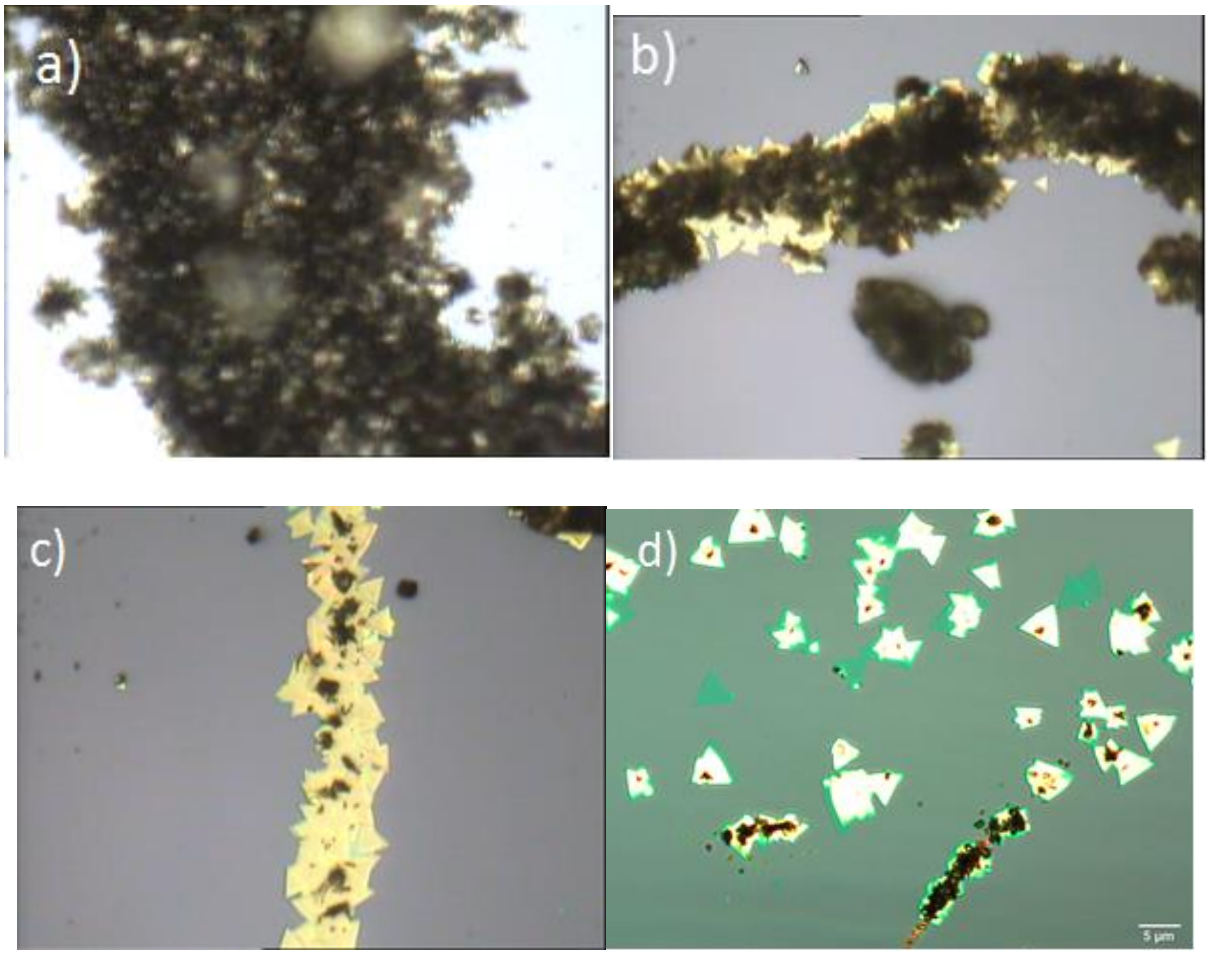

Fig 21: Improvements in CVD growth results in chronological order, with a) being the earliest and d) being the latest

It can be seen in a) that the WS_2 flakes are completely covered in WS_2 particles. Adjustments were made to slowly reduce the growth of these particles. In c), there is minimal particle growth, but the WS_2 flakes still remain very thick. Finally in d), there are some bluish green triangles present, which are the thin WS_2 flakes desired.

Below is an optical image of one of the biggest WS_2 thin flakes grown using the best parameters, approximately 40 μm in length.

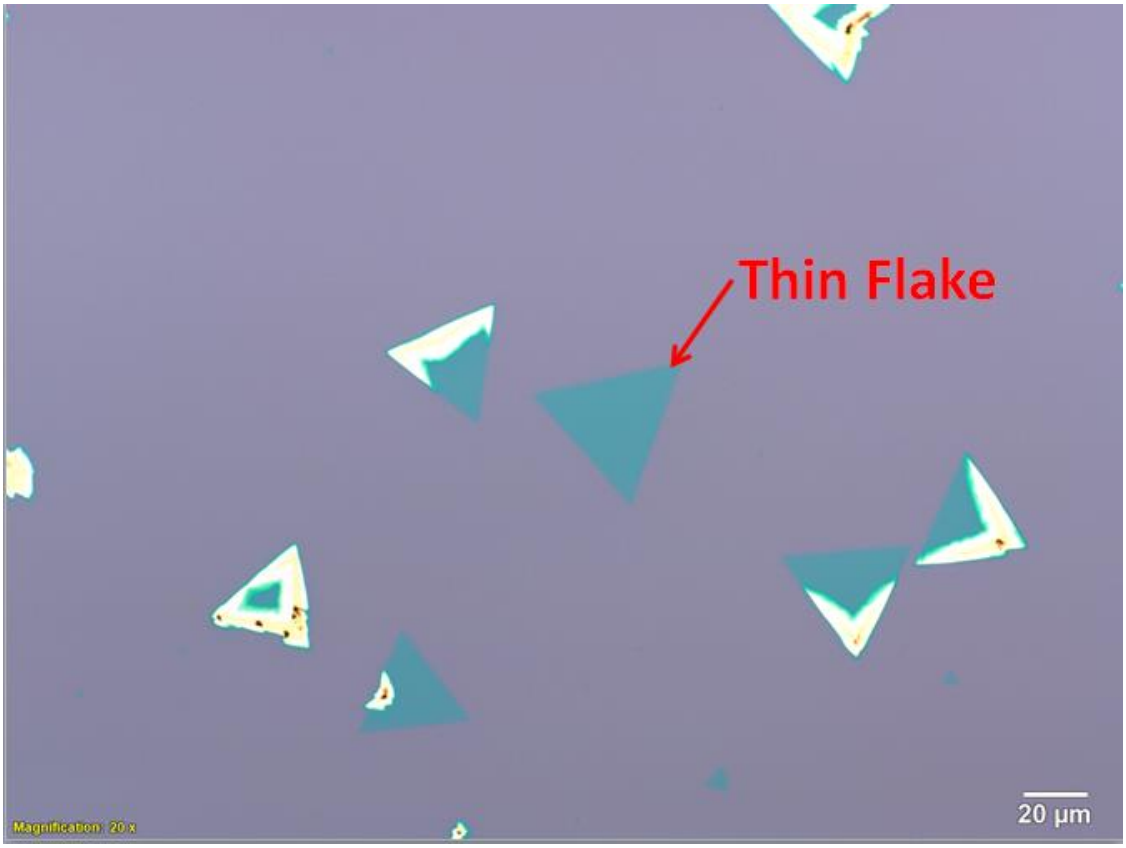

Fig 22: Optical image of thin WS_2 flake

Thin areas of flakes are indicated by a blue colour whereas the thicker areas are indicated by a whiter colour.

4.1.2. Synthesis on sapphire substrate

A majority of knowledge of CVD growth on SiO_2/Si substrate can also be applied to CVD on sapphire substrate. I started off using the growth parameters that Peimyoo et al.[10] used, making adjustments across the duration of my project to optimize it to the tube furnace I was using.

4.1.2.1 Position of substrate

Unlike SiO_2/Si substrate, we found that the optimum position of the sapphire substrate is to be placed face up beside the WO_3 precursor.

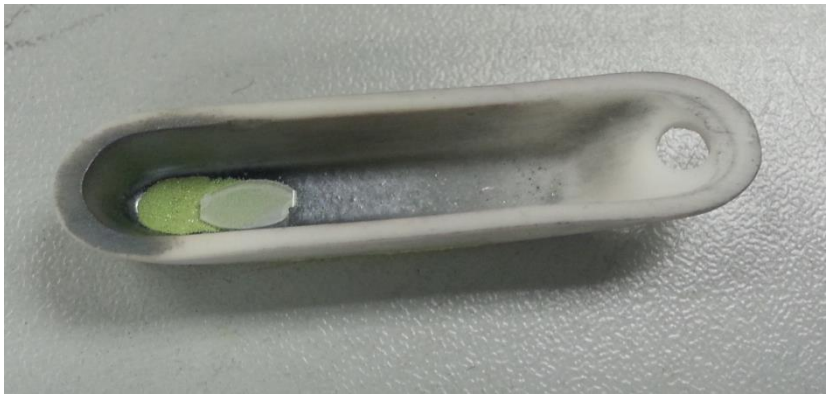

Fig 23: Position of sapphire substrate in ceramic boat

The position of the sapphire was varied along the ceramic boat. It was consistently observed that the edge of the sapphire closest to WO_3 precursor always had the most flake growth. If the substrate was placed further away from the precursor, there would be lesser flakes grown. If the sapphire was placed face down, there will be more WS_2 particles grown. Below is an optical image consisting of thin flakes, thick areas and WS_2 particles.

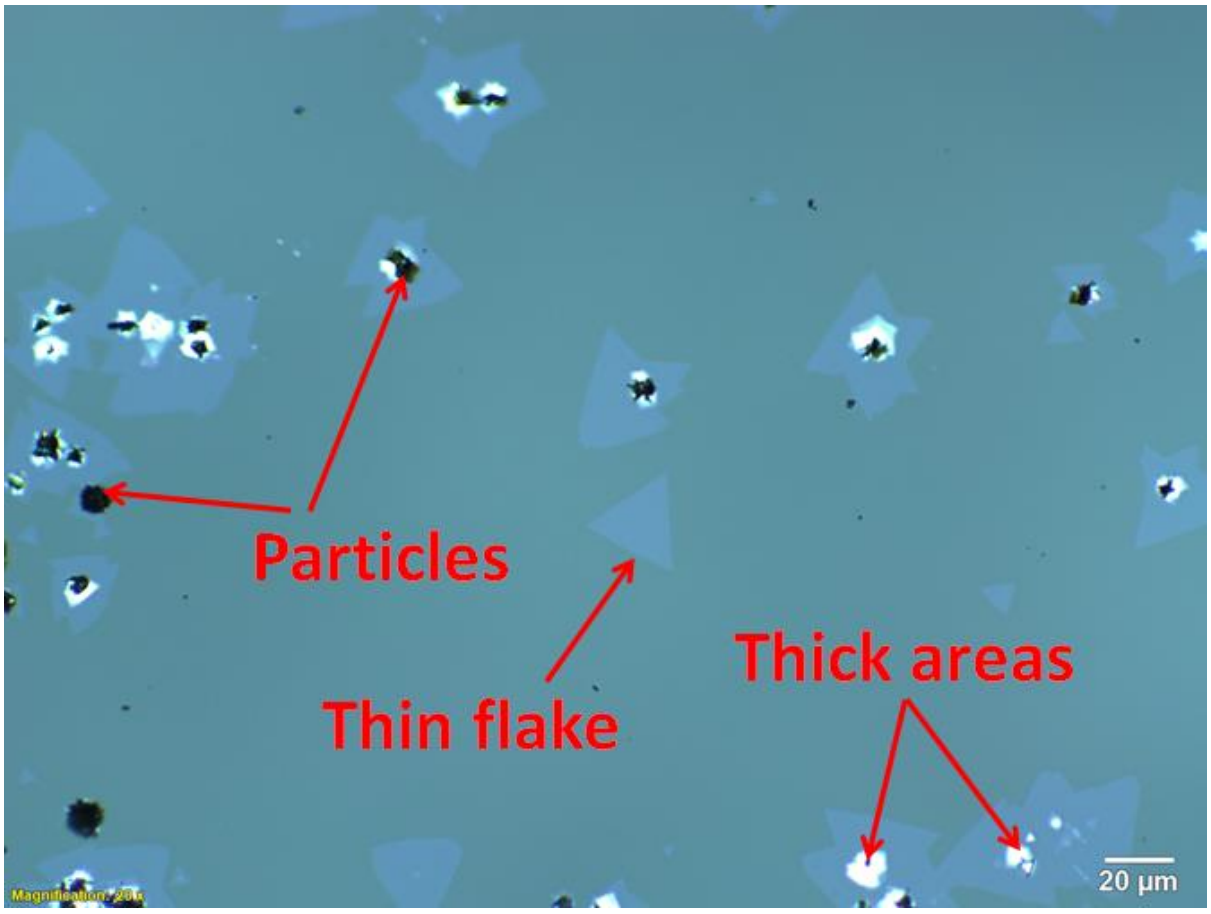

Fig 24: Optical image thin flakes, thick areas and WS_2 particles on sapphire substrate

4.1.2.2. Position of precursor

The WO_3 precursor was always placed at the corner of the ceramic boat, towards the side downstream of the furnace. Due to the amount of Sulphur precursor and the size of its ceramic boat, the Sulphur precursor always took up the entire ceramic boat. Following the same principle as with CVD using SiO_2/Si, the WO_3 precursor and sapphire was positioned in the centre of the furnace ensuring it experiences the most accurate temperature. Since for this CVD the Sulphur precursor is separately heated by a heating plate, there was no need to adjust the position of it. The Sulphur precursor was placed 25 cm away from the centre of the furnace and the WO_3 precursor.

4.1.2.3. Amount of precursor

Using the same knowledge for growth on SiO_2/Si substrate, I found the optimum amount of precursors used is 20 mg of WO_3 and 200 mg of Sulphur.

4.1.2.4 Temperature

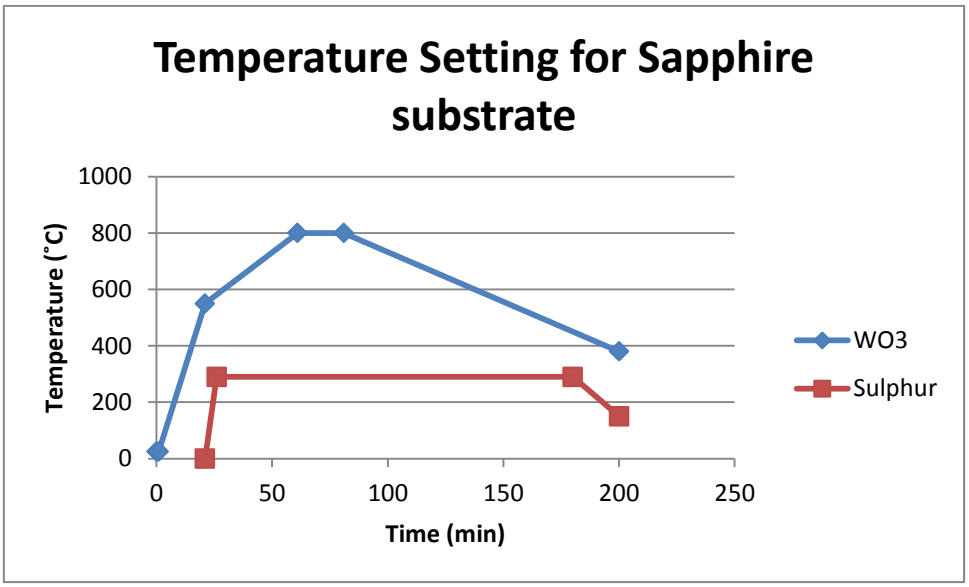

Fig 25: Temperature setting for CVD on sapphire substrate

The temperature is first kept at 25˚C for 1 min to flush out the air, water vapour and other impurities from the chamber. The temperature is then raised to 550˚C at a ramping speed of 25˚C/min for 21mins. When the WO_3 precursor hits 550˚C, the Sulphur precursor begins to heat by a separate heating plate to 290˚C. The temperature of WO_3 precursor then continues to rise to 800˚C at a ramping speed of 6.25˚C/min for 40 min. The growth stage then begins, dwelling at 800˚C for 20 min. This is followed by cooling through the argon gas and natural

cooling. After approximately 3 hours, the WO_3 precursor reaches approximately 400˚C. This is when the heating plate beneath the Sulphur precursor is turned off.

The ramping speed for the WO_3 precursor from 550˚C to 800˚C was varied between 5-10˚C/min. A higher ramping speed caused thicker flake growth. The growth stage temperature was varied between 750-850˚C. Using a higher temperature caused lesser flake growth. However, 750-800˚C seemed to have equally good growth. The growth stage duration was also varied between 10-20 mins. A shorter duration caused lesser flake growth.

4.1.2.5. Gas Supply and Pressure

Through the whole CVD, the chamber is supplied with 200sccm of argon gas at atmospheric pressure. Approximately after 6 hours after the start of the CVD, the chamber will reach between 100-200˚C. The gas supply is turned off and the tube furnace is left to cool by natural cooling.

The argon supply was varied between 100-200sccm. A lower rate would lead to lesser growth of WS_2 flakes.

4.1.2.6. Sulphur-rich environment.

Across the course of my project, the test tube used for CVD was changed a total of 3 times. It was noticed that every time it was changed, the growth of WS_2 flakes would decrease drastically, giving a relatively clean sapphire substrate after CVD. Since this always coincided with the changing of a new test tube, we suspect that a test tube with more condensed Sulphur was better for CVD. A picture of the test tubes used for both CVD processes are shown below.

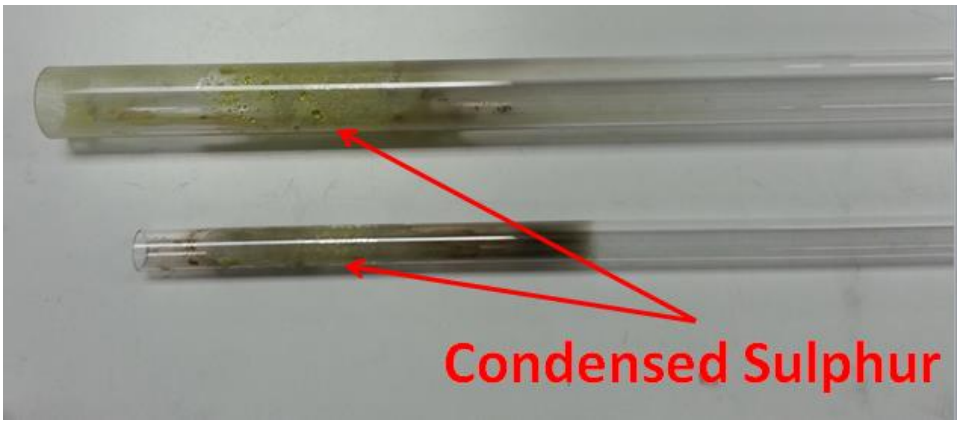

Fig 26: Condensed Sulphur in test tubes used for CVD

The amount of condensed Sulphur is proportional to the number of CVDs it has undergone. It takes approximately 7 CVDs for a new test tube to obtain sufficient condensed Sulphur for the growth of thin WS_2 flakes. I suspect this creates a Sulphur-rich environment for the WO_3 precursor and sapphire substrate, helping the growth of WS_2 thin flakes.

4.1.2.7. Best parameters

In summary, the best parameters I concluded with are as follows.

TMD grown:	WS_2		
Substrate used:	sapphire		
Position of substrate:	Right beside WO_3, facing up		
Position of precursors:	WO3: centre of furnace	Sulphur: 25cm upstream from centre	
Amount of precursor:	Wo3: 20mg	Sulphur: 200mg	
Gas supply & pressure:	Gas: 200sccm argon	Pressure: 1 atm	
Temperature settings			
End temp (°C)	**Ramping Speed (°C/min)**	**Time (min)**	**Heating plate temp (°C)**
25	0	1	0
550	25	22	290 (start when WO3 550°C)
800	6.25	62	290
800	0	82	290
400(approx)	4(approx)	180(approx)	0 (switch off heating plate)

Fig 27: Table of parameters for CVD on sapphire substrate

Compared to the CVD using SiO_2/Si substrates, the improvements in growth were not as obvious across time. The quality of growth on sapphire substrate fluctuated a lot more. However, here are some examples of non-ideal WS_2 flakes.

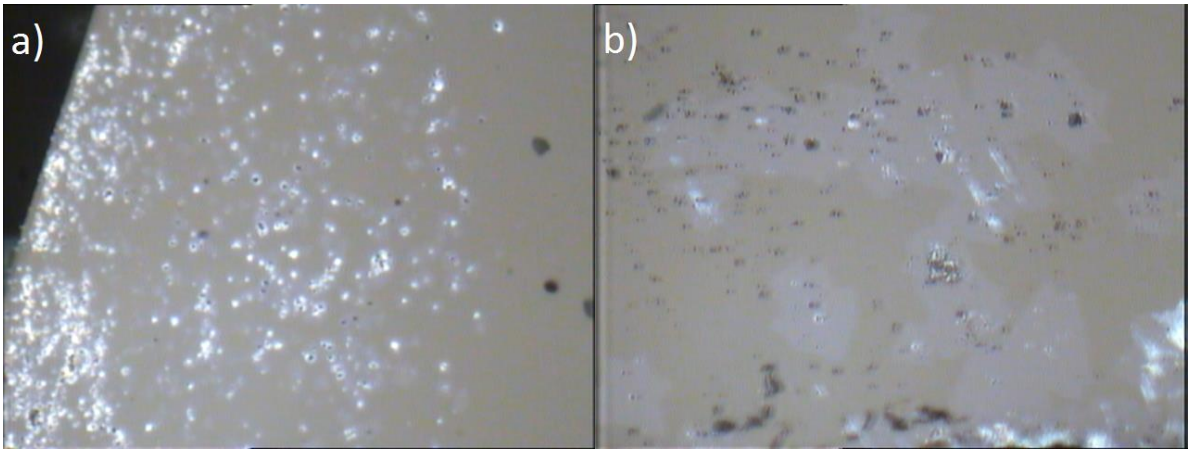

Fig 28: a) Bright areas represent thick areas on the flakes. b) Black WS_2 particles present

The images a) and b) shows an example of a substrate with thick WS_2 flakes and black WS_2 particles respectively. An image using the best growth parameters is shown below.

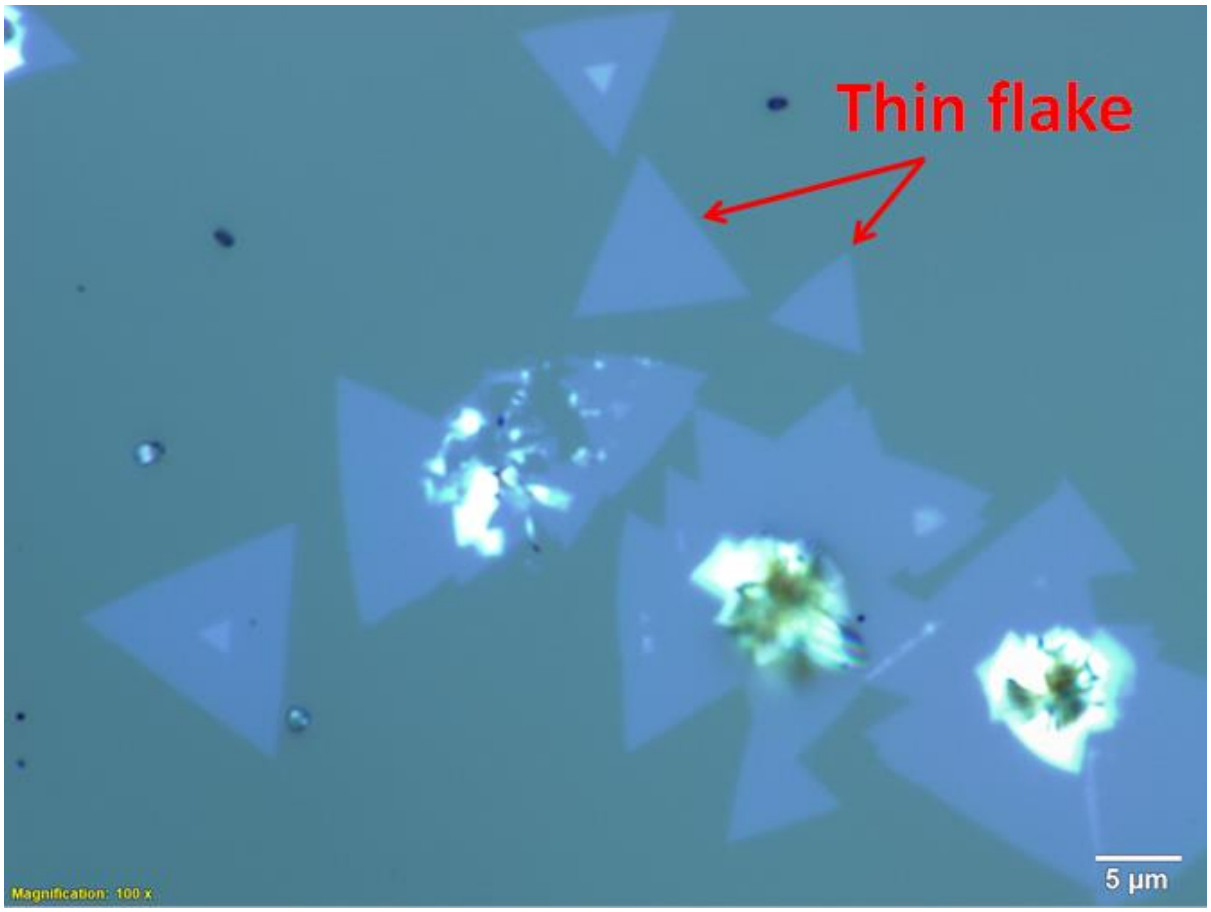

Fig 29: Optical image of thin WS_2 flakes using best parameters

Although there are still some thick areas on the flakes, there some which appear to be uniformly thin, indicated by the arrows in the figure.

4.2. Characterisation of thin WS_2 flakes

The WS_2 flakes synthesized by CVD were then studied using various techniques as mentioned in the Methodology Section earlier. The main focus was the thin WS_2 flakes.

4.2.1. Raman Spectroscopy

Raman Spectroscopy was used mainly for identification of objects rather than the study of the vibrational modes in the WS_2 flake. The Raman Spectroscopy results for thin WS_2 flakes on both sapphire and SiO_2/Si substrates are shown in the graphs below.

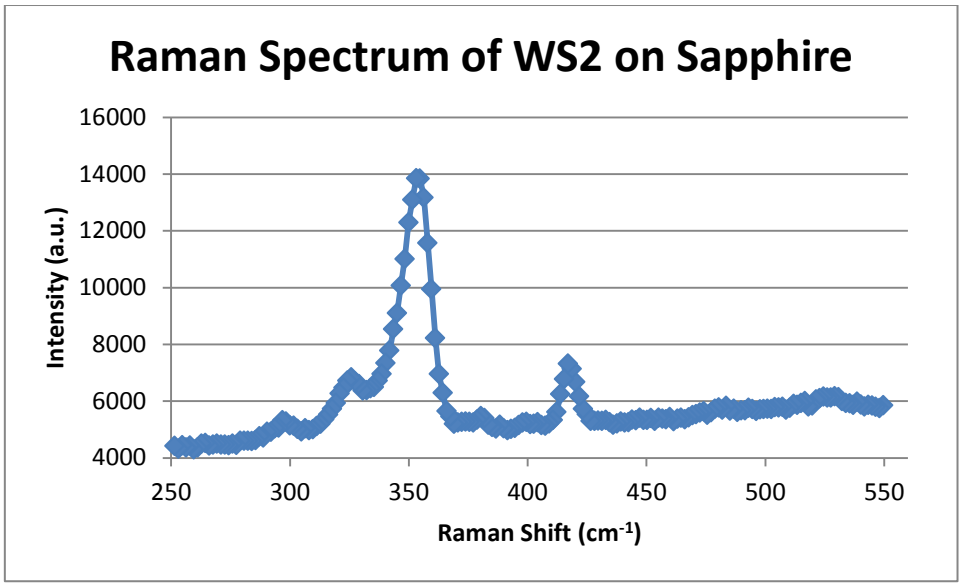

Fig 30: Raman Spectrum of WS_2 flake on sapphire substrate

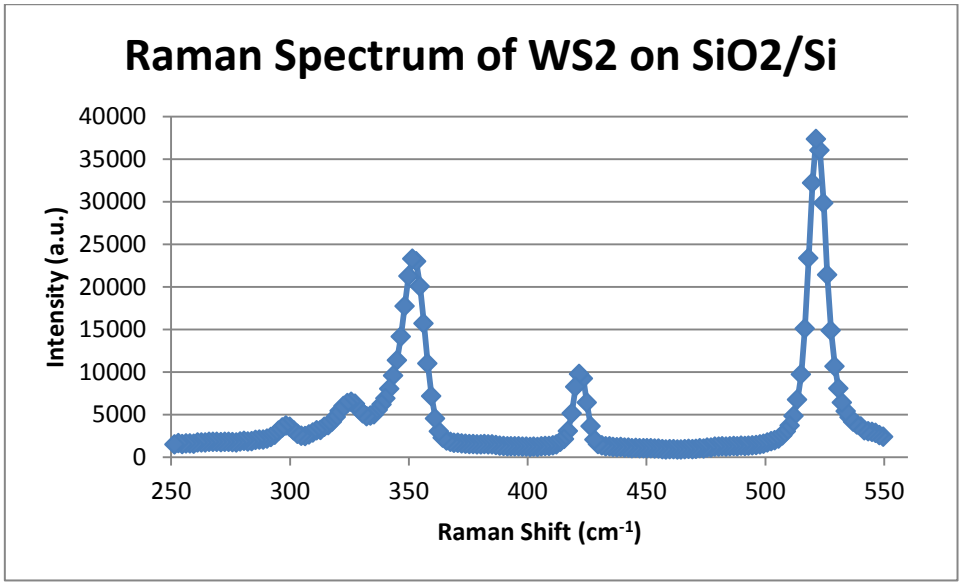

Fig 31: Raman Spectrum of WS_2 flake on SiO_2/Si substrate

It can be seen that the peaks obtained for both Raman spectrums are the same, except that the spectrum taken on SiO_2/Si substrate has an extra peak at 520cm^{-1}. According to Peimyoo et al.[10], this 520cm^{-1} peak corresponds to a vibrational mode in the Silicon present in the

substrate. For WS_2, the 296cm^{-1}, 320cm^{-1} and 417cm^{-1} peaks correspond to the combination mode of 2LA-2E^2_{2g}, combination mode of 2LA-E^2_{2g} and out-of-plane A_{1g} mode respectively. The 350cm^{-1} peak consists of 3 peaks corresponding to the in-plane vibrational E^1_{2g} (M) mode, the second-order mode of longitudinal acoustic phonon 2LA (M) and the in-plane vibrational E^1_{2g} (Γ) mode.[10]

The position of peaks I obtained for WS_2 flakes all have very low percentage discrepancies, the highest being 1.82%. This information is especially useful identifying whether unknown objects observed on the substrate are WS_2.

4.2.2. Photoluminescence Spectroscopy

PL is used mainly to determine the bandgap of thin WS_2 flakes. Below is the PL Spectroscopy results obtained for a thin WS_2 flake on SiO_2/Si substrate.

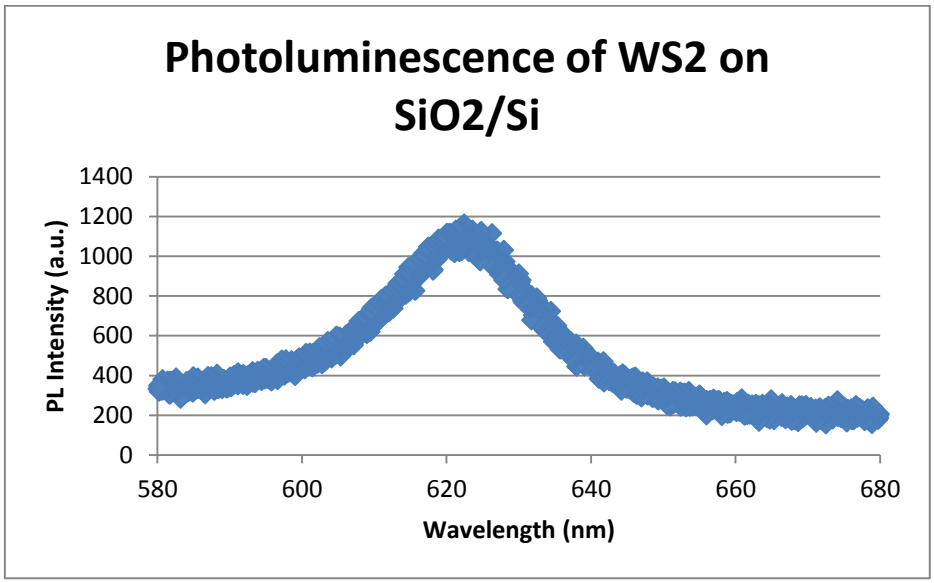

Fig 32: PL Spectrum of WS_2 flake

The wavelength of the PL peak obtained ranges between 620-625nm. This wavelength corresponds to red light, which agrees with the results obtained in the Fluorescence Microscopy I performed. The energy of a photon of wavelength 625nm is 1.98eV. This agrees with Zhu et al.'s[15] A exciton emission of 1.98eV at room temperature. This shows that the bandgap present in thin WS_2 flakes is 1.98eV, assuming it has a perfectly direct bandgap.

4.2.3. Atomic Force Microscopy (AFM)

The AFM machine used had relatively high noise level during the measurements. This can be seen in the amplitude of fluctuations in height relative to the step height corresponding to the transition from the WS_2 flake to the substrate, especially for the WS_2 flake on SiO_2/Si. The steps are identified by a steep decrease in height which corresponds to the position of the edge of the flake along the line of measurement. Using tapping mode AFM for thin WS_2 flakes, I obtained the following results shown below.

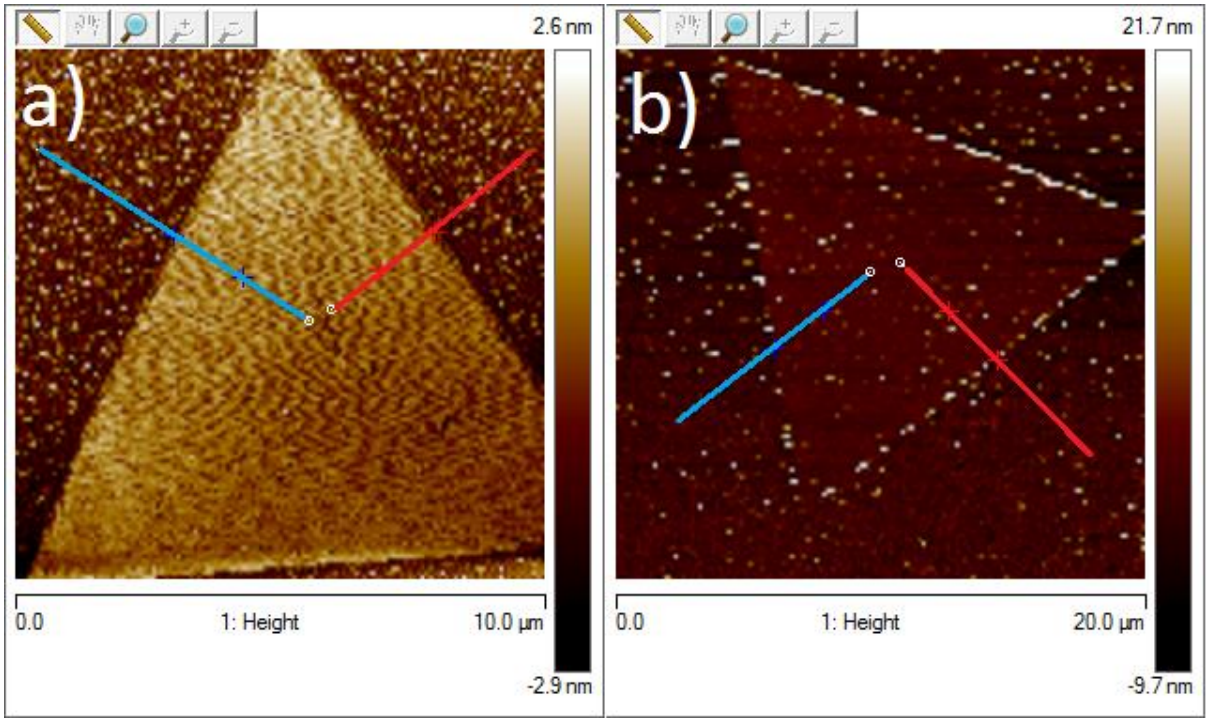

Fig 33: AFM results for WS_2 flake on a) sapphire and b) SiO_2/Si

The morphology along the 2 lines is shown in the graphs below.

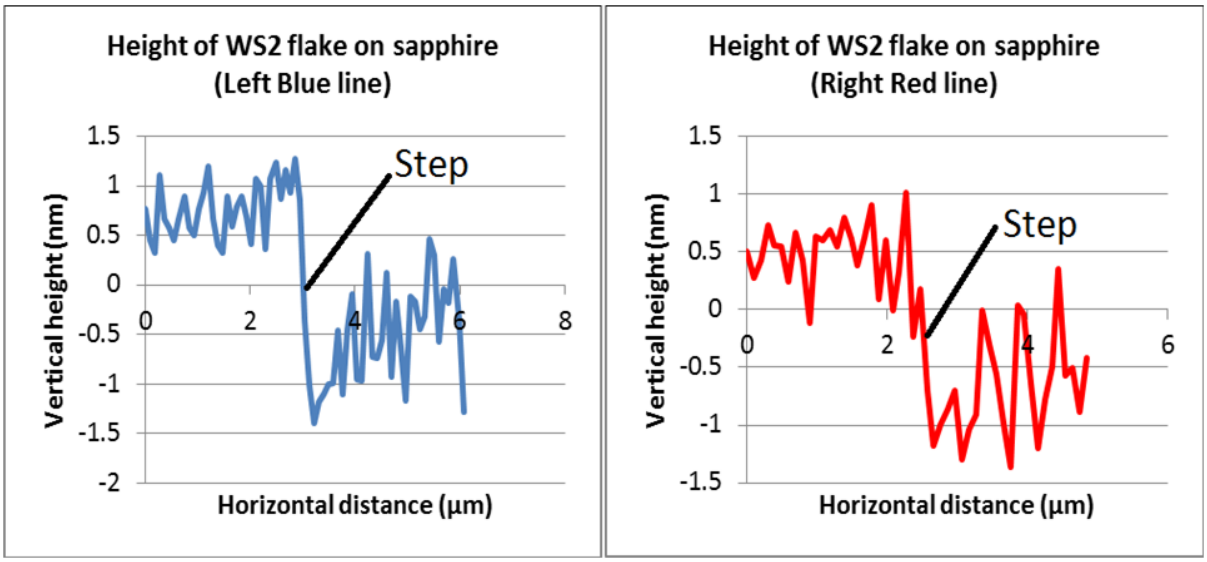

Fig 34: Graphs of morphology for blue and red lines on sapphire

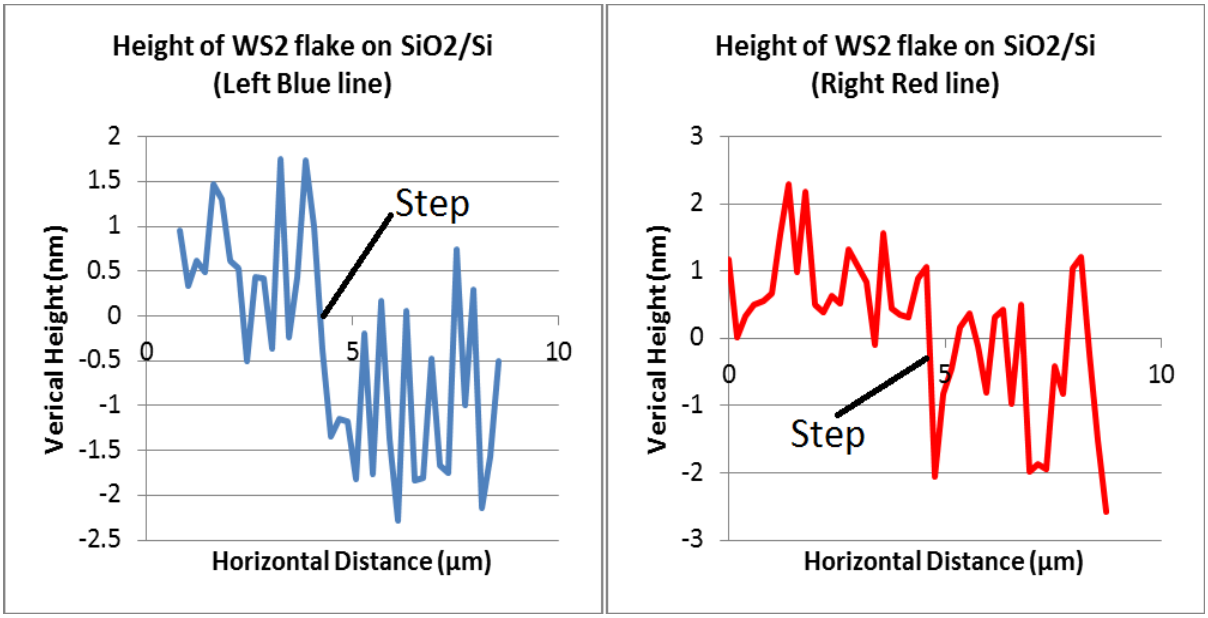

Fig 35: Graphs of morphology for blue and red lines on SiO_2/Si

For each of the graphs, the height values are split into 2 groups, namely the values before the step and after the step. Each step in labelled in the graphs. The values that are within the steps are excluded from calculations. For each group of height values, the average is calculated. The difference between the 2 averages is calculated to be the thickness of the WS_2 flake. The 2 thicknesses of the WS_2 flake on sapphire are calculated to be 1.30nm for the blue line and

1.13nm for the red line. The 2 thicknesses for the WS_2 flake on SiO_2/Si are calculated to be 1.72nm for the blue line and 1.43nm for the red line.

The thickness of 1 layer of WS_2 is approximately 0.7nm.[10] With this knowledge, the WS_2 flake on sapphire is 1-2 layers and the flake on SiO_2/Si is 2-3 layers.

4.2.4. Fluorescence Microscopy

Fluorescence microscopy was performed using white, blue and green light. The images obtained are shown below.

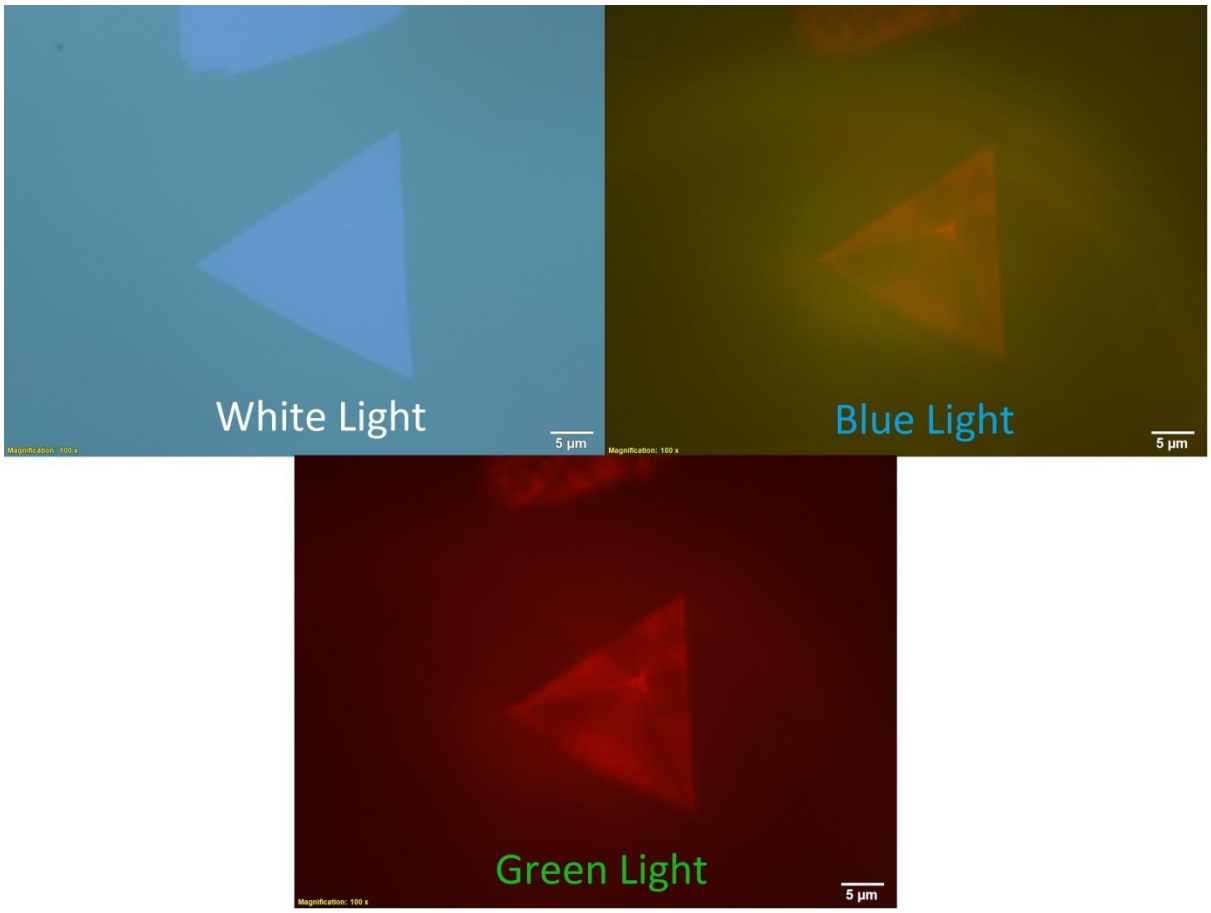

Fig 36: Fluorescence Microscopy results for WS_2 flake on Sapphire

From the results of PL spectroscopy, we found that the PL exhibited corresponded with red light. This agrees with the fluorescence seen from the WS_2 flake on sapphire. It was evident that when using green excitation light, the fluorescence exhibited was stronger in intensity compared to that of blue excitation light, despite the fact that blue light has a higher energy

photon than green light. This shows that green light is closer to the excitation maximum than blue light.

It can be seen that the fluorescence exhibited on the flake has a certain pattern. It is suspected that this pattern reveals the grain boundaries present in the WS_2 flake, which is not visible under white light.

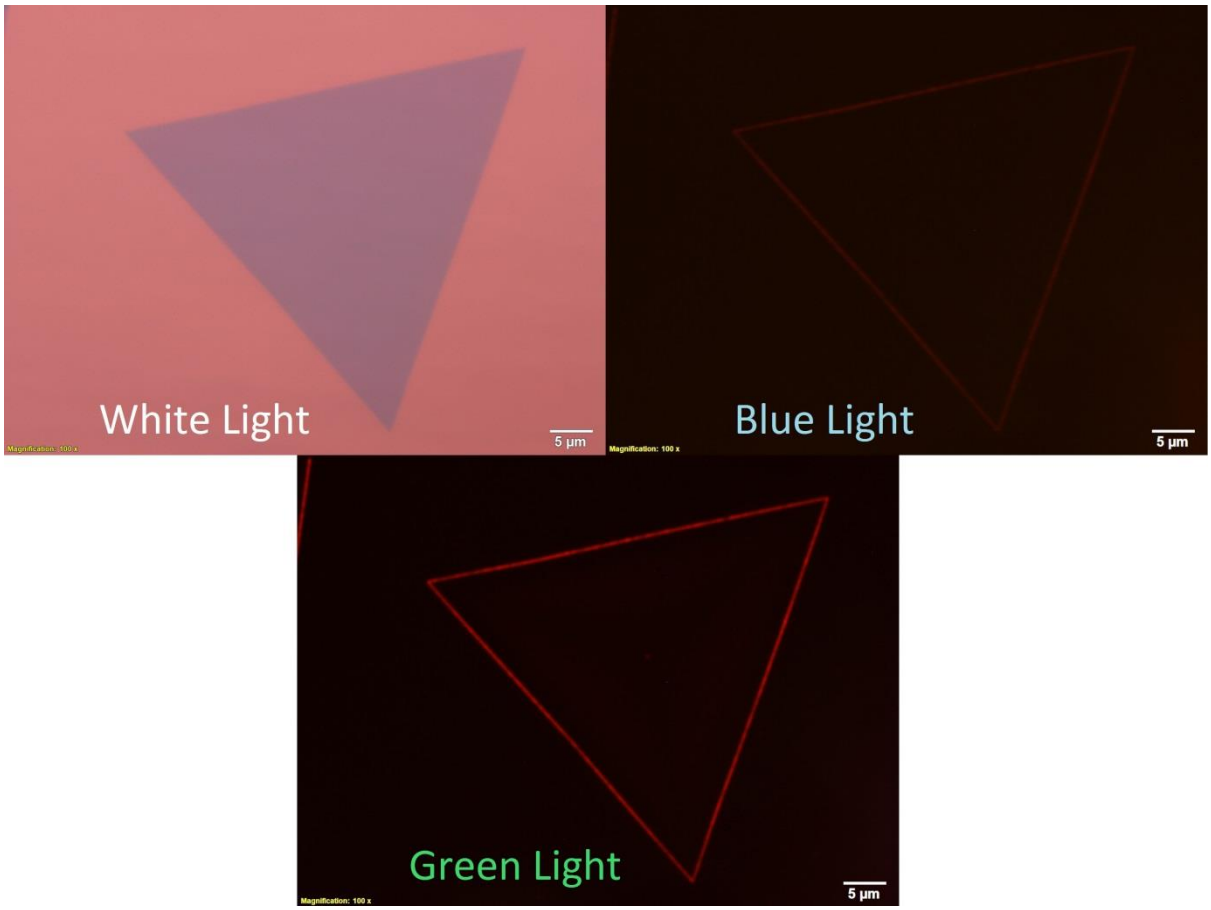

Fig 37: Fluorescence Microscopy results for WS_2 flake on SiO_2/Si

The fluorescence present on the WS_2 flake on SiO_2/Si substrate differs very much from that on sapphire. It is clearly seen that the edges exhibit a lot more fluorescence compared to the rest of the flake area. There are a few possible reasons for this.

One possibility is that the Sulphur precursor was not separately heated at a lower temperature. Heating the Sulphur precursor in the tube furnace gives rise to a relatively unstable supply of Sulphur in the chamber, resulting in non-uniform growth and PL,[10] where the PL is exhibited more at the edges. This is very similar to the CVD carried out for SiO_2/Si in my project. For the CVD using SiO_2/Si, the Sulphur precursor was placed in the tube

furnace, whereas for the CVD using sapphire, the Sulphur precursor was heated at a constant temperature outside the tube furnace.

Another possibility is that the edges of the WS_2 flake on SiO_2/Si are thinner than the rest of the flake. Fluorescence microscopy was done on another region of the SiO_2/Si substrate and the images are shown below.

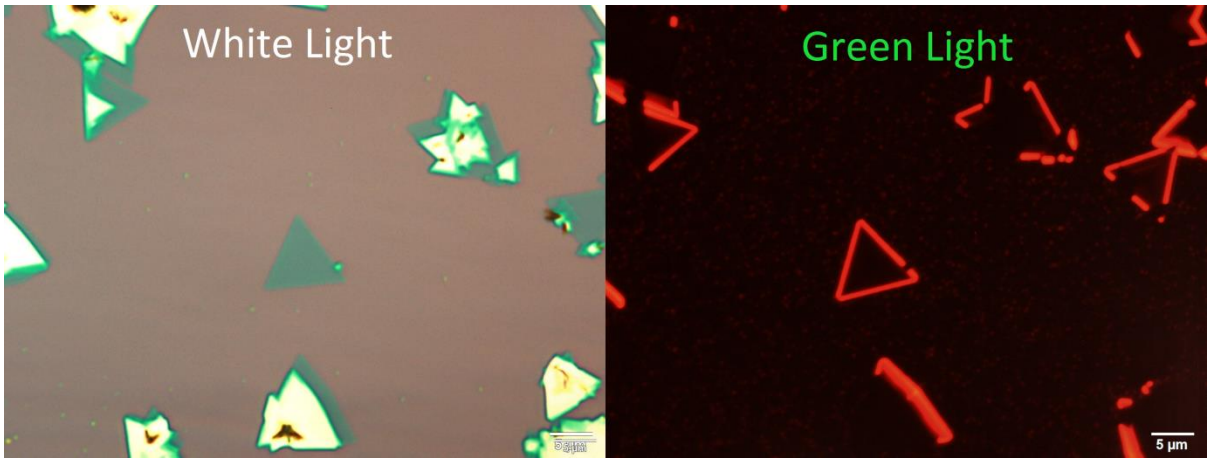

Fig 38: Fluorescence Microscopy of WS_2 flakes on SiO_2/Si substrate

Although the position of the substrate was moved a bit between photos, it can be seen that only the edges of thin areas of the WS_2 flakes exhibited fluorescence. This agrees with Peimyoo et al. which states that intensity of PL decreases with increasing thickness of WS_2 flakes, indicating the transformation from direct to indirect bandgap. With this knowledge, it could be the case that for the thin flakes, only the edges are thin enough to exhibit fluorescence.

Attempts to use the AFM to analyse the height profile and determine whether there was indeed a thickness difference at the edge of the flake, but the noise level present made it difficult to do so.

4.3. Optoelectronic Device

Using the CVD method, other TMDs flakes such as WSe_2 monolayers was also synthesized. According to Fang et al.[16], single layered WSe_2 has an ambipolar behavior, meaning that it can behave as either a p-type or n-type semiconductor, depending on the material used for the electrode. If the electrode used is Palladium (Pd), WSe_2 will behave as a p-type semiconductor. According to Allen et al.[17], CdS can be used as an n-type semiconductor.

According to Dong et al.[18], CdSe can also be used as an n-type semiconductor. According to Baglio et al.[19], WS_2 could be used as either p-type or n-type semiconductor. With this knowledge, I wanted to construct a *p-n* junction using WSe_2 and $CdS_{0.8}Se_{0.2}$.

Synthesizing WSe_2 flakes on sapphire substrate uses the same CVD technique as that of WS_2 flakes on sapphire. A heating plate was used to separately heat the Selenium precursor outside the tube furnace. According to Liu et al.[20], the bandgap for monolayer WSe_2 is approximately 1.6eV, which corresponds to photons of 775nm wavelength, which is in the infra-red spectrum.

An optoelectronic device was fabricated using a sapphire substrate with WSe_2 flakes grown on it and a $CdS_{0.8}Se_{0.2}$ nanowire. This optoelectronic device helps us to incorporate the WSe_2 flake and $CdS_{0.8}Se_{0.2}$ nanowire into a circuit through the use of electrodes, while keeping the WSe_2 flake and $CdS_{0.8}Se_{0.2}$ nanowire exposed so that lasers can be incident onto it. This helps in the study of the optoelectronic properties of the heterostructure junction between WSe_2 and $CdS_{0.8}Se_{0.2}$. This optoelectronic device is fabricated through the Electron Beam Lithography (EBL) method.

For the measurements of IV graphs and Ivst graphs, different lasers of wavelengths 543nm (green), 405nm (blue), and 660nm (red) were used separately. The power for all 3 lasers used was 1.00mW with a spot size of approximately $2mm^2$.

4.3.1. IV graphs

The IV graphs were measured for dark current (with no laser incident upon it) and with lasers of different wavelengths.

The IV graphs are shown below.

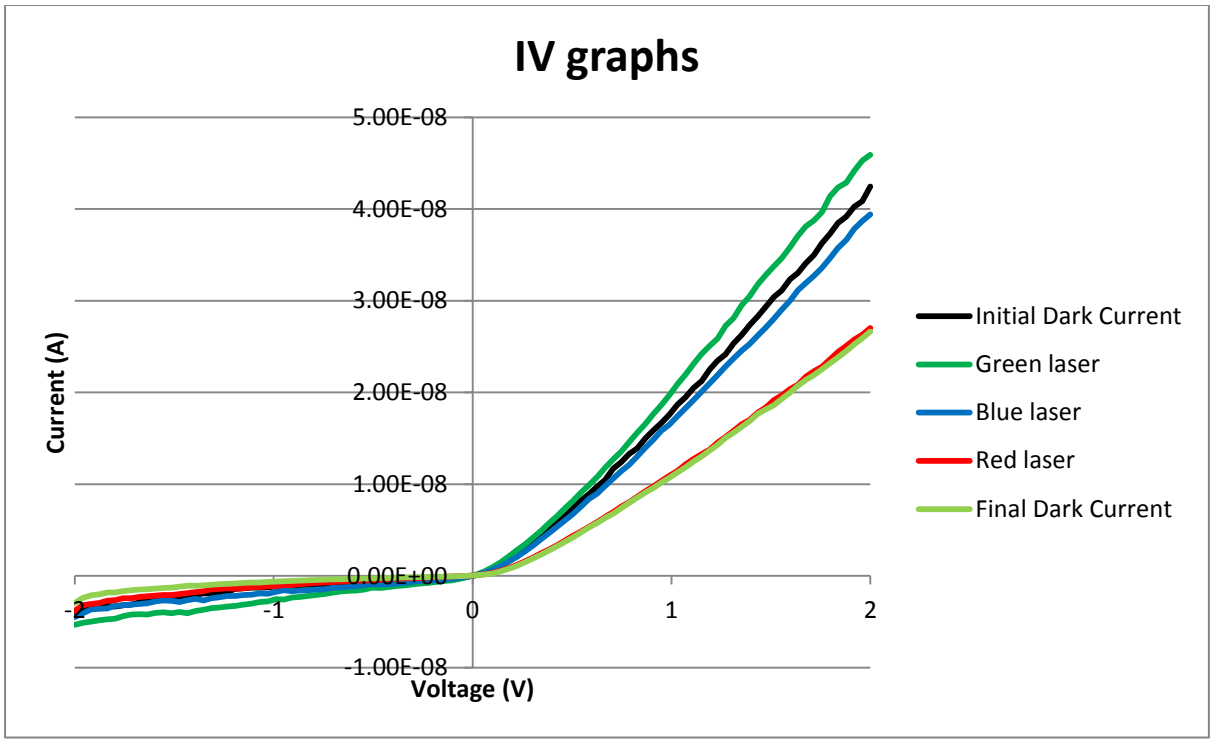

Fig 39: IV Graphs

The shape if these IV graphs show that this heterostructure junction behaves as a *p-n* junction. The order of IV graphs obtained were initial dark current first, followed by green, then blue then red laser. It can be seen that the initial dark current is higher than the current using blue and red lasers. I found this strange and went ahead to obtain another dark current IV graph after the above IV graphs were taken. This is labelled as Final Dark Current.

It can be seen that after the IV measurements using lasers, the dark current has significantly decreased. This degradation in conductivity could be caused by the incident lasers or exposure to air. This makes it difficult to determine the additional current when a laser is incident upon the junction. This additional current is called the photocurrent.

4.3.2. Current against time (Ivst) graphs

To overcome this problem, another technique is used. Instead of measuring current against voltage, a measurement of current against time is made while keeping the potential difference constant at 2V. During the measurement, the laser is allowed to incident upon the device for 5

seconds, followed by blocking the laser for another 5 seconds. These “ON” and “OFF” states are repeated approximately 5 times. These Ivst graphs are shown below.

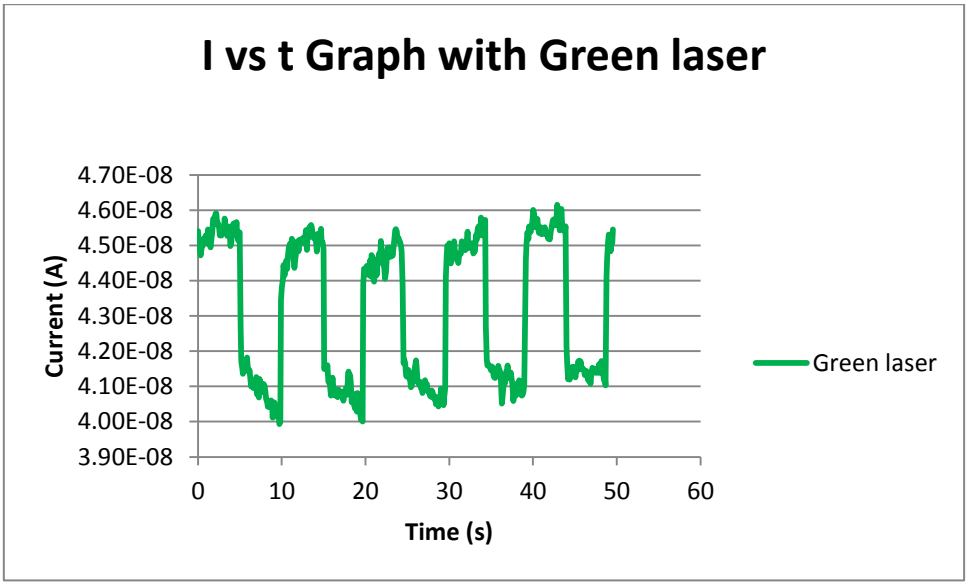

Fig 40: Current against time graph using Green laser

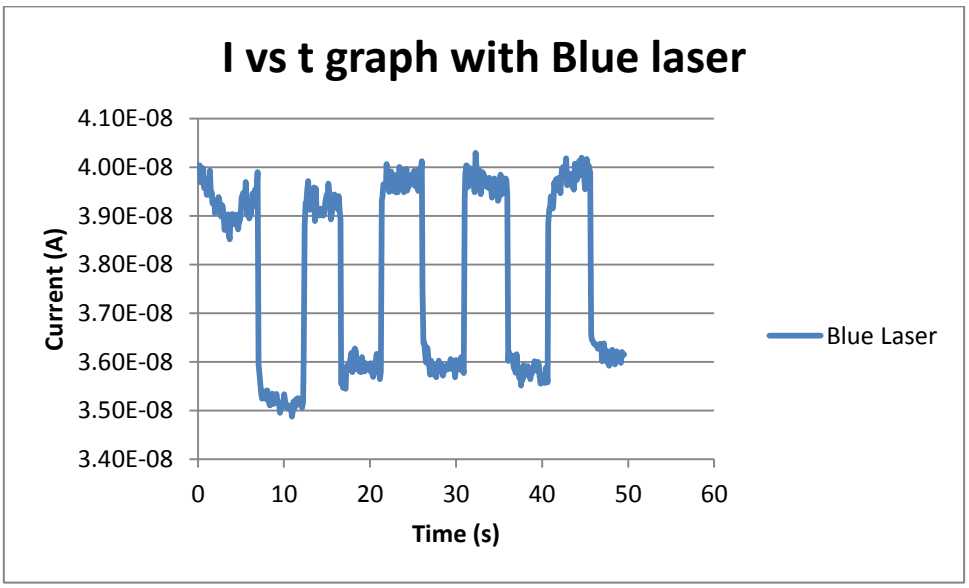

Fig 41: Current against time graph using Blue laser

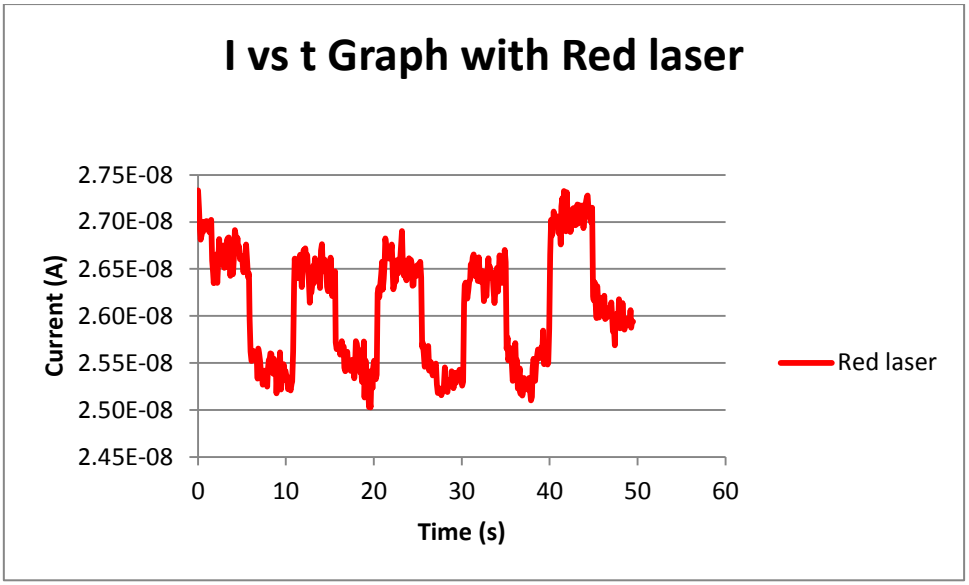

Fig 42: Current against time graph using Red laser

It can be clearly seen that there is a photocurrent present for all 3 lasers. All the current values in the "ON" state were averaged to give the current under illumination, I_{illum}. All the current values in the "OFF" state were averaged to give the dark current, I_{dark}. The difference between these 2 averages would be the calculated photocurrent. All current values that were ambiguous to whether they were during the "ON" or "OFF" periods were excluded from calculation. This was done for all 3 graphs of different lasers.

Following this, the Photoresponsivity (R_{res}), External Quantum Efficiency (EQE) and Photodetectivity (D*) was calculated for the different lasers.

4.3.2.1. Photoresponsivity

Photoresponsivity is a measure of the amount of photocurrent generated in response to the amount of power incidence upon the device from the excitation laser.

$$R_{res} = \frac{I_{pho}}{P_{opt}} = \frac{I_{illum} - I_{dark}}{(P_{inc})S}$$

Where I_{pho} is the photocurrent, P_{opt} is the light power. S is the effective area of the optoelectronic device, which consists of the WS_2 flake and the section of the $CdS_{0.8}Se_{0.2}$ nanowire which carries the current. P_{inc} is the power density of the illumination.[21] S is calculated to be approximately $5.0*10^{-11}m^2$ and P_{inc} is approximately $500W/m^2$. Using this

information, R_{res} was calculated to be $0.161AW^{-1}$ for green laser, $0.150AW^{-1}$ for blue laser and $0.0442AW^{-1}$ for red laser.

A similar experiment was carried out by a senior student in NUS, where the electrodes were placed on a single WSe_2 flake on her device. A laser of wavelength 532nm was used for global irradiation with a power of 2.8mW and a spot size of ~$2mm^2$. The photoresponsivity calculated was $25mAW^{-1}$. It can be seen that by adding a $CdS_{0.8}Se_{0.2}$ nanowire, the heterostructure has enhanced the overall photoresponsivity compared to if just WSe_2 was used. These results are currently in the process of being published.

According to Kang et al.[22], the photoresponsivity of WSe_2 was calculated to be approximately $4.5mAW^{-1}$ when using a excitation wavelength of 785nm and power of 1mW. Although the excitation wavelength used is not the same as the ones used in my project, this photoresponsivity value supports that the use of heterostructure is probably better than non-heterostructure.

4.3.2.2.External Quantum Efficiency

External Quantum Efficiency (EQE) shows the number of additional charge carriers generated per photon that incidence upon the device. EQE is calculated using the equation below.

$$EQE = \frac{hcR_{res}}{e\lambda}$$

Using the photoresponsivity, R_{res}, the EQE can be calculated. h is Planck's constant, c is the speed of light, e is the charge of an electron and λ is the excitation wavelength.[23] The EQE calculated is 0.492 for green laser, 0.458 for blue laser and 0.135 for red laser.

The EQE calculated from using a single WSe_2 flake was 0.0583.

4.3.2.3. Photodetectivity

Photodetectivity is a measure of the performance of a photon sensitive device. Photodetectivity is calculated using the equation below.[22]

$$D^* = \frac{R_{res} S^{\frac{1}{2}}}{(2eI_{dark})^{\frac{1}{2}}}$$

The photodetectivity calculated to be $9.90*10^6$ Jones for green laser, $9.98*10^6$ Jones for blue laser and $3.46*10^6$ Jones for red laser.

From the photoresponsivity, EQE and photodetectivity calculated, it can be seen that the green laser of 543nm yields the best results compared to the other 2 wavelengths. This is interesting because even though blue photons possess a higher energy per photon, the green laser exhibits better results. This show that wavelength 543nm is closer to the excitation maximum peak than 405nm for either the WSe_2 or $CdS_{0.8}Se_{0.2}$ or both. I did not identify the extent of the individual contributions from the different components of the device. This will be discussed further in the later section 5.2. of "future work".

5. Conclusion

5.1. Summary of project

In my project, I managed to synthesize thin WS_2 flakes on sapphire and SiO_2/Si substrates. This was done by optimising the parameters for the Chemical Vapour Deposition process. The parameters that were varied for the parameter search were the position of the substrate, position and amount of precursor, temperature settings, gas supply rate, pressure and a few others. The parameters used on SiO_2/Si could also be used for Si_3N_4 substrate.

Next, the characteristics of the WS_2 flakes were studied using different techniques. Raman Spectroscopy was used for identification of WS_2. Photoluminescence Spectroscopy was used for determining the bandgap of WS_2, which is approximately 1.98eV, corresponding to a wavelength of 625nm. Atomic Force Microscopy was used to measure the morphology and thickness of the WS_2 flakes, where it was found that the WS_2 flakes grown on sapphire substrate were between 1-2 layers and the flakes on SiO_2/Si substrate were between 2-3 layers. Fluorescence Microscopy is used to observe which areas on the WS_2 flake exhibit fluorescence. It was observed that WS_2 flakes on sapphire substrate generally exhibited fluorescence throughout its whole area, whereas the thin WS_2 flake on SiO_2/Si exhibited fluorescence only at the edges.

Finally, with the use of a heterostructure optoelectronic device using a WSe_2 flake and $CdS_{0.8}Se_{0.2}$ nanowire , the current against voltage (IV) graphs and current against time (Ivst) graphs were obtained using lasers of 3 different wavelengths. The Ivst measurements were done for “ON” and “OFF” states where the laser was unblocked and blocked respectively. Photoresponsivity, External Quantum Efficiency (EQE) and Photodetectivity were calculated for each of the lasers. It can be seen that the excitation wavelength of 543nm was the closest to the excitation maximum compared to 405nm and 660nm wavelengths for either WSe_2 or $CdS_{0.8}Se_{0.2}$. Cross referencing the Photoresponsivity of WSe_2 flakes, the heterostructure junction shows promising improvements in optoelectronics.

5.2. Possible Future Work

Due to time constrains, there are a few more things related to my project that can be explored and studied in the future.

Instead of synthesizing the 2 materials of the heterostructure separately and then manually stacking them, another suggestion is that a 2 step CVD process can be used synthesize the heterostructure. This means that after synthesizing a TMD flake for example, the substrate can be used for the synthesis of the next TMD, where the second TMD can possibly grow on top of the first TMD. This might give rise to different or enhanced optoelectronic properties.

It was observed that only the edges of the thin WS_2 flakes grown on SiO_2/Si substrate exhibited fluorescence whereas the other areas exhibited much less. More research can be done on this. A more accurate AFM with less noise can be used to measure a very detailed height profile at the edge of the flake to see if indeed the edge is thinner than the rest of the flake.

It was found that the heterostructure junction exhibits photocurrent when exposed to lasers. However, global irradiation was used, which means that the extent of photocurrent contributions from the different components on the device is unknown. Instead of using a broad beam laser, a focused laser can be used to irradiate only specific components on the optoelectronic device. This way, the contributions photocurrent from each component can be determined.

To expand on my findings, another identical optoelectronic device can be constructed, except that instead of having heterostructure junction of WSe_2 and $CdS_{0.8}Se_{0.2}$, only WSe_2 is used. This way, a direct comparison can be done between using a single material and a heterostructure junction, performing the exact measurements on each device.

Different combinations of heterostructures can be used too. There are other TMDs available such as MoS_2 and $MoSe_2$. CdS and CdSe can also be used instead of CdS_xSe_{1-x}.

References:

1) Meric, I., Baklitskaya, N., Kim, P., & Shepard, K. L. (2008, December). RF performance of top-gated, zero-bandgap graphene field-effect transistors. In*IEEE International Electron Devices Meeting* (pp. 1-4).
2) Dean, C. R., Young, A. F., Meric, I., Lee, C., Wang, L., Sorgenfrei, S., ... & Hone, J. (2010). Boron nitride substrates for high-quality graphene electronics.*Nature nanotechnology*, *5*(10), 722-726.
3) Yun, W. S., Han, S. W., Hong, S. C., Kim, I. G., & Lee, J. D. (2012). Thickness and strain effects on electronic structures of transition metal dichalcogenides: 2H-M X 2 semiconductors (M= Mo, W; X= S, Se, Te).*Physical Review B*, *85*(3), 033305.
4) Eda, G., Yamaguchi, H., Voiry, D., Fujita, T., Chen, M., & Chhowalla, M. (2011). Photoluminescence from chemically exfoliated MoS2. *Nano letters*,*11*(12), 5111-5116.
5) Mueller, T., Furchi, M. M., Pospischil, A., & Polyushkin, D. K. (2014, December). Nanophotonics with two-dimensional atomic crystals. In *Electron Devices Meeting (IEDM), 2014 IEEE International* (pp. 5-5). IEEE.
6) Tongay, S., Zhou, J., Ataca, C., Lo, K., Matthews, T. S., Li, J., ... & Wu, J. (2012). Thermally driven crossover from indirect toward direct bandgap in 2D semiconductors: MoSe2 versus MoS2. *Nano letters*, *12*(11), 5576-5580.
7) Chhowalla, M., Shin, H. S., Eda, G., Li, L. J., Loh, K. P., & Zhang, H. (2013). The chemistry of two-dimensional layered transition metal dichalcogenide nanosheets. *Nature chemistry*, *5*(4), 263-275.
8) Ling, X., Lee, Y. H., Lin, Y., Fang, W., Yu, L., Dresselhaus, M. S., & Kong, J. (2014). Role of the seeding promoter in MoS2 growth by chemical vapor deposition. *Nano letters*, *14*(2), 464-472.
9) Lee, Y. H., Zhang, X. Q., Zhang, W., Chang, M. T., Lin, C. T., Chang, K. D., ... & Lin, T. W. (2012). Synthesis of Large-Area MoS2 Atomic Layers with Chemical Vapor Deposition. *Advanced Materials*, *24*(17), 2320-2325.
10) Peimyoo, N., Shang, J., Cong, C., Shen, X., Wu, X., Yeow, E. K., & Yu, T. (2013). Nonblinking, intense two-dimensional light emitter: Monolayer WS2 triangles. *ACS nano*, *7*(12), 10985-10994.
11) Gfroerer, T. H. (2000). Photoluminescence in analysis of surfaces and interfaces. *Encyclopedia of Analytical Chemistry*.
12) Choi, J. O., Moore, J. A., Corelli, J. C., Silverman, J. P., & Bakhru, H. (1988). Degradation of poly (methylmethacrylate) by deep ultraviolet, x-ray, electron beam, and proton beam irradiations. *Journal of Vacuum Science & Technology B*, *6*(6), 2286-2289.
13) Junpeng, L., Cheng, S., Minrui, Z., Mathews, N., Hongwei, L., Gin Seng, C., ... & Chorng Haur, S. (2011). Facile One-Step Synthesis of CdS x Se1–x Nanobelts with Uniform and Controllable Stoichiometry. *The Journal of Physical Chemistry C*, *115*(40), 19538-19545.

14) Rong, Y., Fan, Y., Koh, A. L., Robertson, A. W., He, K., Wang, S., ... & Warner, J. H. (2014). Controlling sulphur precursor addition for large single crystal domains of WS 2. *Nanoscale*, *6*(20), 12096-12103.
15) Zhu, B., Zeng, H., Dai, J., Gong, Z., & Cui, X. (2014). Anomalously robust valley polarization and valley coherence in bilayer WS2. *Proceedings of the National Academy of Sciences*, *111*(32), 11606-11611.
16) Fang, H., Chuang, S., Chang, T. C., Takei, K., Takahashi, T., & Javey, A. (2012). High-performance single layered WSe2 p-FETs with chemically doped contacts. *Nano letters*, *12*(7), 3788-3792.
17) Bard, A. J., & Wrighton, M. S. (1977). Thermodynamic Potential for the Anodic Dissolution of n-Type Semiconductors A Crucial Factor Controlling Durability and Efficiency in Photoelectrochemical Cells and an Important Criterion in the Selection of New Electrode/Electrolyte Systems. *Journal of the Electrochemical Society*, *124*(11), 1706-1710.
18) Yu, D., Wang, C., & Guyot-Sionnest, P. (2003). n-Type conducting CdSe nanocrystal solids. *Science*, *300*(5623), 1277-1280.
19) Baglio, J. A., Calabrese, G. S., Harrison, D. J., Kamieniecki, E., Ricco, A. J., Wrighton, M. S., & Zoski, G. D. (1983). Electrochemical characterization of p-type semiconducting tungsten disulfide photocathodes: efficient photoreduction processes at semiconductor/liquid electrolyte interfaces. *Journal of the American Chemical Society*, *105*(8), 2246-2256.
20) Liu, W., Kang, J., Sarkar, D., Khatami, Y., Jena, D., & Banerjee, K. (2013). Role of metal contacts in designing high-performance monolayer n-type WSe2 field effect transistors. *Nano letters*, *13*(5), 1983-1990.
21) Lu, J.P., Liu, H., Deng, S., Zheng, M., Wang, Y., Kan, J.A.V., Sing, H.T., Zhang, X., Chorng, H.S., Subodh, G.M. (2014). Highly sensitive and multispectral responsive phototransistor using tungsten-doped VO_2 nanowires. *Nanoscale*, 6,7619-7627
22) Kang, D. H., Shim, J., Jang, S. K., Jeon, J., Jeon, M. H., Yeom, G. Y., ... & Park, J. H. (2015). Controllable Nondegenerate p-Type Doping of Tungsten Diselenide by Octadecyltrichlorosilane. *ACS nano*, *9*(2), 1099-1107.
23) Baugher, B. W., Churchill, H. O., Yang, Y., & Jarillo-Herrero, P. (2014). Optoelectronic devices based on electrically tunable pn diodes in a monolayer dichalcogenide. *Nature nanotechnology*, *9*(4), 262-267.